




## RESEARCH ARTICLE

# Automated facies identification by Direct Push-based sensing methods (CPT, HPT) and multivariate linear discriminant analysis to decipher geomorphological changes and storm surge impact on a medieval coastal landscape

Hanna Hadler<sup>1</sup>  | Andreas Vött<sup>1</sup> | Timo Willershäuser<sup>1</sup> | Dennis Wilken<sup>2</sup> | Ruth Blankenfeldt<sup>3</sup> | Claus von Carnap-Bornheim<sup>3</sup> | Kurt Emde<sup>1</sup> | Peter Fischer<sup>1</sup>  | Ulf Ickerodt<sup>4</sup> | Stefanie Kloöß<sup>4</sup> | Bente Majchczack<sup>2</sup>  | Lea Obrocki<sup>1</sup> | Wolfgang Rabbel<sup>2</sup>

<sup>1</sup>Institute of Geography, Johannes Gutenberg-Universität Mainz, Mainz, Germany

<sup>2</sup>Institute of Geosciences, Christian-Albrechts-Universität Kiel, Kiel, Germany

<sup>3</sup>Zentrum für Baltische und Skandinavische Archäologie Schleswig, Schleswig, Germany

<sup>4</sup>Archäologisches Landesamt Schleswig-Holstein, Schleswig, Germany

## Correspondence

Hanna Hadler, Institute of Geography, Johannes Gutenberg-Universität Mainz, 55099 Mainz, Germany.  
Email: hadler@uni-mainz.de

## Funding information

Deutsche Forschungsgemeinschaft, Grant/Award Numbers: HA 7647/1-1, RA 496/26-2, VO 938/21-1; Research Foundation

## Abstract

In AD 1362, a major storm surge drowned wide areas of cultivated medieval marshland along the north-western coast of Germany and turned them into tidal flats. This study presents a new methodological approach for the reconstruction of changing coastal landscapes developed from a study site in the Wadden Sea of North Frisia. Initially, we deciphered long-term as well as event-related short-term geomorphological changes, using a geoscientific standard approach of vibracoring, analyses of sedimentary, geochemical and microfaunal palaeoenvironmental parameters and radiocarbon dating. In a next step, Direct Push (DP)-based Cone Penetration Testing (CPT) and the Hydraulic Profiling Tool (HPT) were applied at vibracore locations to obtain *in situ* high-resolution stratigraphic data. In a last step, multivariate linear discriminant analysis (LDA) was successfully applied to efficiently identify different sedimentary facies (e.g., fossil marsh or tidal flat deposits) from the CPT and HPT test dataset, to map the facies' lateral distribution, also in comparison to reflection seismic measurements and test their potential to interpolate the borehole and CPT/HPT data. The training dataset acquired for the key site from coring and DP sensing finally allows an automated facies classification of CPT/HPT data obtained elsewhere within the study area. The new methodological approach allowed a detailed reconstruction of the local coastal landscape development in the interplay of natural marsh formation, medieval land reclamation and storm surge-related land losses.

## KEYWORDS

Cone Penetration Testing (CPT), Hydraulic Profiling Tool (HPT), North Frisia, storm surge, Wadden Sea

## 1 | INTRODUCTION

The Wadden Sea of North Frisia (Germany, Figure 1) is protected as a national park and part of the UNESCO natural world heritage 'Wadden Sea' because of its unique ecosystem (UNESCO, 2009). Yet,

the present-day tidal flats are not only an outstanding natural landscape, but also the result of major geomorphological changes associated with intense anthropogenic impacts on the environment. In fact, they are the relic of a former cultural landscape drowned by extreme storm surges since the Middle Ages (Newig, 2014).

This is an open access article under the terms of the Creative Commons Attribution-NonCommercial License, which permits use, distribution and reproduction in any medium, provided the original work is properly cited and is not used for commercial purposes.

© 2021 The Authors. *Earth Surface Processes and Landforms* published by John Wiley & Sons Ltd.

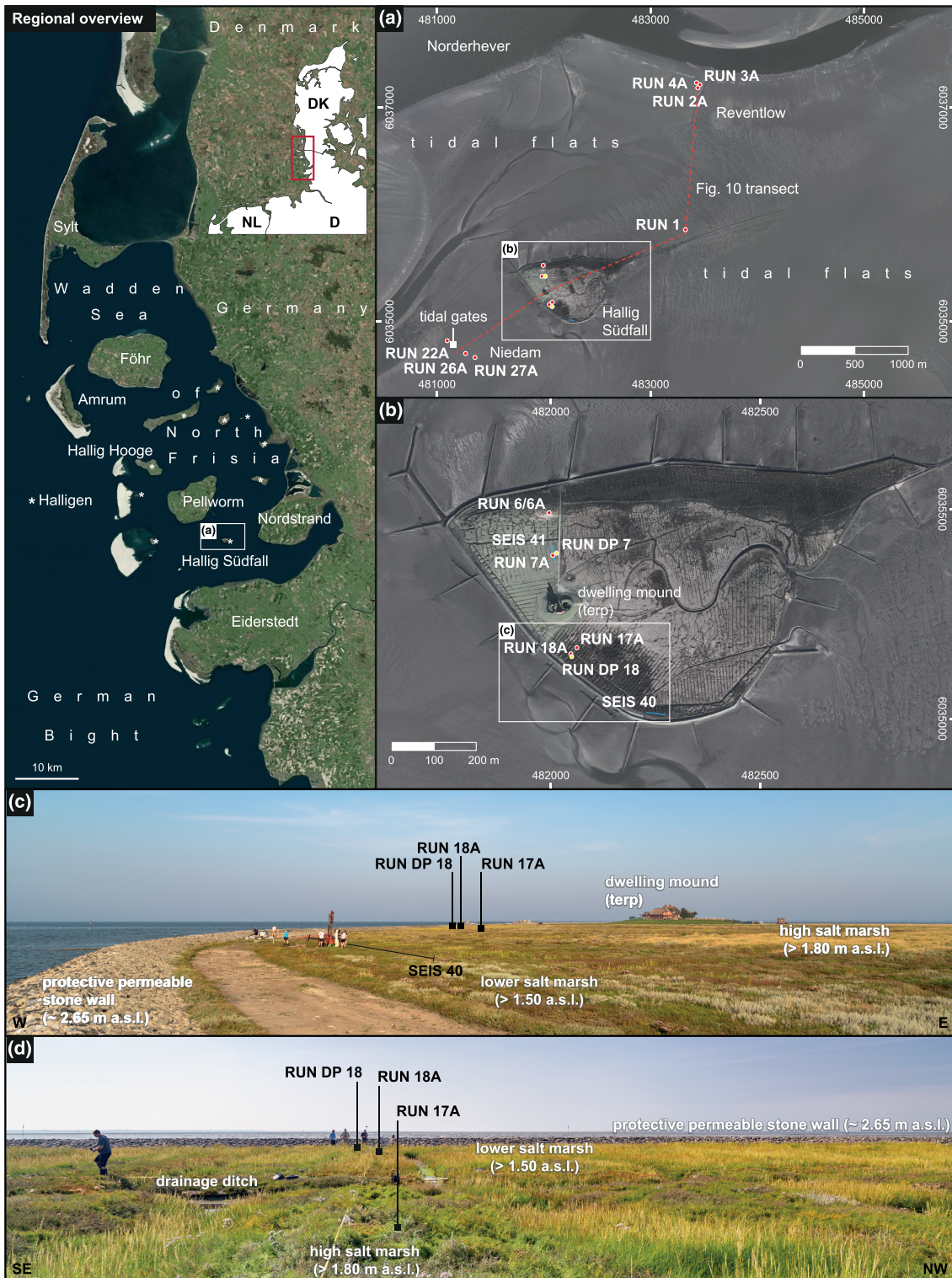


**FIGURE 1** Aerial image of the North Frisian Wadden Sea, Hallig Südfall and surrounding tidal flats (a, b) showing vibracoring (red dots), direct push sensing (yellow dots) sites and seismic profiles (blue line). The key site on Hallig Südfall is a lower to high salt marsh environment (c, d), crossed by drainage ditches and fascines. The outer edges of the Hallig are protected by a permeable stone wall that prevents erosion but allows sea water to flow through. Aerial images: Bing aerial maps, 2021; LKN, 2018; photographs: H. Hadler, 2016, 2019 [Color figure can be viewed at [wileyonlinelibrary.com](https://onlinelibrary.com)]

As a result of post-glacial sea-level rise, this coastal landscape has gradually changed during the Holocene (Behre, 2008; Dittmer, 1952; Meijles et al., 2018). While barrier islands and back barrier tidal flats dominate the morphology of the adjacent German, Danish or Dutch Wadden Sea regions (e.g., Bungenstock & Schäfer, 2009; Fruergaard et al., 2015; Lindhorst et al., 2008; Vos & Knol, 2015), Pleistocene

outcrops and an extensive spit system cut North Frisia off from the open sea. A brackish shallow water back barrier environment developed in today's Wadden Sea region, only little influenced by the North Sea through tidal inlets (Hoffmann, 2004).

From 2000 BC onwards, permanent siltation of this lagoon-like system formed wide fenlands and marshes, traversed by different

types of waterbodies such as lakes and estuarine channels. In the mid-first millennium BC, the marine influence became almost negligible (Bantelmann, 1967; Hoffmann, 2004) but this amphibious coastal landscape was still hardly accessible for man. It was not before the 12th century AD that the extensive and systematic reclamation of low-lying marshes and fenlands began to significantly change the so far natural coastal landscape (Bantelmann, 1975; Kühn & Panten, 1989; Kühn, 2007).

Intense draining of marshland and extensive peat extraction for melioration and salt production significantly lowered the land surface, sometimes even below mean high water (MHW; Bantelmann, 1967; Fischer & Müller, 1936; Hoffmann, 2004). This effect is reinforced by regional sediment compaction (Higelke et al., 1982), while at the same time dike building along the coast increased the tidal range (Petersen & Rohde, 1977). To the low-lying cultivated areas, these early dikes barely offered protection against strong storm surges (Kühn & Panten, 1989). So, when in AD 1362 a major storm surge hit North Frisia (the so-called *1st Grote Mandränke* or *2nd Marcellus' flood*), large coastal areas between Eiderstedt and Föhr were flooded and permanently destroyed (Figure 1 Regional overview). In places, the North Sea advanced as far as 25 km inland, reaching the Pleistocene moraines (Newig, 2004).

After AD 1362, reclamation of lost land was only accomplished in some places (e.g., Pellworm, Nordstrand; cf. Heimreich, 1982) while wide areas had turned into shallow water tidal flats. New land reclamation projects (e.g., between Nordstrand and Pellworm; Heimreich, 1982) point to locally increased siltation and marsh formation but another major storm surge in AD 1634 (the so-called *2nd Grote Mandränke* or *Burchardi flood*) led to the final establishment of the Wadden Sea. The present-day coastal landscape of North Frisia thus reflects the effects of intense anthropogenic interference with coastal marshlands that significantly increased their vulnerability against extraordinary storm surges.

Until today, our knowledge of the extensive destruction in AD 1362 mostly relies on historic descriptions and maps or archaeological evidence from the present tidal flats. Geoscientific evidence, however, is rare as working in the Wadden Sea is challenging and suitable geoarchives preserving post-AD 1362 sediments are few (Hadler et al., 2018b). To decipher the palaeogeographical development until and since medieval times, the method of choice would be a standard approach of coring, analyses of sediment samples, evaluation of proxy data and (radiocarbon) dating, widely used in geoscientific studies (Brückner & Gerlach, 2020; Goldberg & Macphail, 2006). Additionally, statistical analyses of proxy data (e.g., linear discriminant analysis, LDA) may be used for automated facies identification (Vött et al., 2002). Yet, a classical palaeogeographical reconstruction across the > 1500 km<sup>2</sup> wide excavation reserve 'Wadden Sea' by core analyses would be a life's work (Ickerodt et al., 2017). A large-scale geoscientific investigation of North Frisia's coastal history requires an easier applicable, less time consuming and cost-efficient research approach.

During the last years, Direct Push (DP)-based *in situ* sensing methods like electrical conductivity (EC) logging, Cone Penetration Testing (CPT), the Hydraulic Profiling Tool (HPT) or Colour Logging Tool (CLT) are increasingly applied in geoscientific and geoarchaeological research and successfully used for palaeogeographical reconstructions (Koster, 2016; Hausmann et al.,

2018; Fischer et al., 2020; Hadler et al., 2020; Rabiger-Völlmer et al., 2020; Verhegge & Delvoie, 2021, Verhegge et al., 2021). Combined with geophysical prospection data, the site-specific data from DP-based *in situ* sensing methods can even be spatially extrapolated (Bates et al., 2007; Fischer et al., 2016; Obrocki et al., 2020). Measured parameters do, however, not provide direct information on the texture, geochemical parameters or microfaunal content of a sediment – that is, the sedimentary facies – but merely reflect 'technical' parameters like the EC, mechanical behaviour (CPT) or porosity (HPT) (Obrocki et al., 2020). For a palaeogeographical reconstruction including not only sedimentary but also environmental changes, DP-based *in situ* sensing data must therefore be combined with site-specific stratigraphic data from core analyses, acting as a local reference. Yet, for a detailed and reliable reconstruction, one must also be able to interpret DP-based *in situ* data for locations without an adjacent core stratigraphy.

The major aims of this study are therefore

- (i) to decipher major landscape changes and storm surge impacts in the Wadden Sea of North Frisia (Germany) using a geoscientific standard approach of vibracoring, palaeoenvironmental parameter analysis and radiocarbon dating at a test site with well-known historical context,
- (ii) to evaluate the reliability of geomorphological results in comparison with historical and archaeological evidence,
- (iii) to develop and test a new methodological approach for fast and efficient prospection of local stratigraphies based on an automated facies interpretation combining data from CPT, the HPT and LDA as well as geophysical prospection (reflection seismics) and
- (iv) to evaluate the potential of this new approach and its applicability to the wider Wadden Sea region and other study areas.

## 2 | REGIONAL SETTING AND HISTORICAL BACKGROUND

Only little is known about North Frisia's coastal landscape in medieval times, although its remnants are still preserved in the tidal flats (e.g., around Hallig Hooge or Pellworm). Highest densities of cultural remains occur around the study area of Hallig Südfall (Figures 1 and 2; Kühn, 2007) and comprise, for example, the largest group of medieval dwelling mounds ever found offshore North Frisia. Radiometric and dendrochronological age determination of a former dike by associated tidal gates date the cultural remains that are likely related to a medieval settlement called Rungholt, to the 12th to 14th centuries AD (Hadler et al., 2018a; Kühn, 2007; Newig & Hauptenthal, 2016).

The medieval remains (Figure 2) – all widely exposed in the 1920s (Busch, 1923, 1962) – offered valuable archaeological insights into the once cultivated marshland and fenland (Hadler et al., 2018c; Ickerodt et al., 2017; Kühn, 2007). Yet, from a geomorphological point of view, the tidal flats represent an incomplete sedimentary archive inappropriate for palaeogeographical reconstructions, since post-AD 1362 sediments have either never been accumulated or have already been eroded by recent tidal dynamics. The most promising geoarchive that can be used to decipher the landscape evolution of North Frisia's Wadden Sea region from pre-medieval times until today are most likely the Halligen Islands (Figure 1 Regional overview).

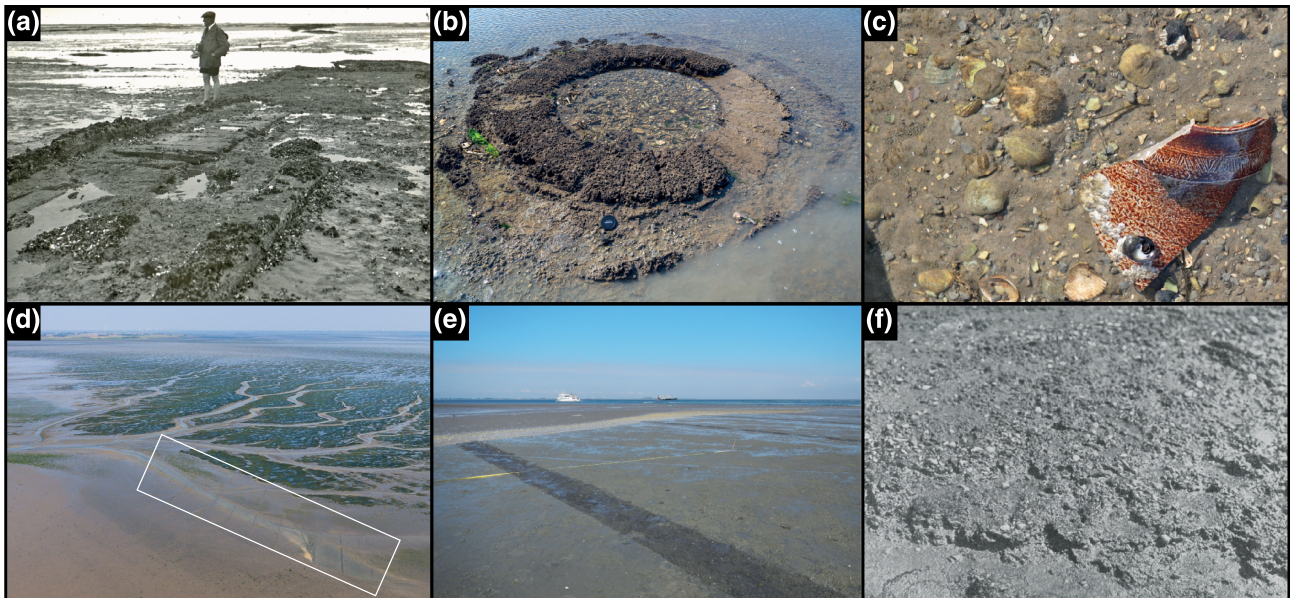


**FIGURE 2** Medieval cultural remains preserved in the Wadden Sea around Hallig Südfall include, for example, wooden tidal gates (a), sod cisterns (b) or sherds and bones (c). Drainage ditches are also widely preserved and at times exposed by tidal inlets (d). Acting as sediment traps, some are filled with a mixture of marine and terrestrial sediments (e.g., shells, peat) and anthropogenic artefacts (e.g., sherds, bones), likely deposited by the AD 1362 storm surge (e). Similar deposits near Hallig Südfall were described by Peters (1932) as ‘transgressive conglomerate’ and equally interpreted as storm surge deposit (f) (Hadler & Vött, 2016). Photographs: NordseeMuseum Husum, 2017; H. Hadler, 2019; T. Willershäuser, 2019; H. Hadler, 2016; Peters, 1932 [Color figure can be viewed at [wileyonlinelibrary.com](http://wileyonlinelibrary.com)]

Unlike the neighbouring islands of Sylt, Amrum or Föhr, the Halligen comprise no Pleistocene core. Until today, they are mostly unprotected by dikes so that the formation of marshland by frequent flooding and siltation still continues (Schindler et al., 2014b, 2014a). Some of these small marsh islands are remains of the formerly widespread medieval marsh land, while others have only been forming since Medieval times. Hallig Südfall, for example, is known to lie in an area previously settled and drowned by medieval storm surges. The post-medieval age of the Hallig is implied by several archaeological observations, where exposed fossil marshland, peat extraction pits or drainage ditches extend from the tidal flats underneath the marsh islands (e.g., Busch, 1923, 1963a; Möller, 1926). It must therefore be assumed that Hallig Südfall belongs to one of few sites where sediments from before and after the AD 1362 storm surge are quite likely preserved and can be used for a detailed reconstruction of the coastal landscape development.

With a historically well-known event chronology, Südfall also represents a geo-archive well-suitable to correlate geoscientific with historical and archaeological data and to test the new methodological approach of facies interpretation from DP-based CPT and HPT sensing. For this study, we chose a location in the south-western part of the marsh island (Figure 1c). With elevations between +1.51 and +1.80 m above sea level (a.s.l.) the sites lie in the range of local MHW (+1.56 m a.s.l., tide gauge *Südfall Fahrwasserkannte*; BSH, 2020a). Nowadays, the study area is protected by a permeable stone rampart (approximately +2.65 m a.s.l.) that prevents erosion from wave action but allows sea water coming in through shallow ditches (so-called *Grüppen*) during high tide (Figure 1c,d). Further coastal protection measures comprise fascines that extend across the recent marsh surface. Average absolute flooding frequencies per year range from 300 (+1.50 m a.s.l.) to 105 (+1.80 m a.s.l.). Approximately 7.7

times a year, high water exceeds the stone rampart, while storm surges occur 3.7 times on average (frequencies calculated from perennial tide gauge *Everschop* for 1977–2018; LKN, 2019). The recent vegetation is dominated by *Spartina anglica* (cord grass) and *Salicornia europaea* (glasswort), accompanied by *Aster tripolium* (sea aster), *Halimione portulacoides* (sea purslane) and *Atriplex littoralis* (grass-leaved orache), typical of the pioneer zone and lower saltmarsh, respectively (Kremer, 2001).

### 3 | METHODS

This study uses vibracoring, palaeoenvironmental parameter (PEP) analyses of sediment samples and radiocarbon dating, to decipher the sedimentary record of the Hallig Südfall geo-archive and to reconstruct its palaeogeographical evolution. DP-based CPT and the HPT provide additional high-resolution stratigraphic parameters that were subsequently used in a LDA to test their potential for automated facies differentiation. For a potential spatial extrapolation of facies, reflection seismics were carried out near and across the borehole and CPT/HPT sites.

#### 3.1 | Vibracoring

Two vibracores (RUN 17A, RUN 18A; Table 1) were drilled using closed steel augers with plastic liners of 5 cm diameter. The maximum coring depth was 7 m b.s. (below surface) or −5.49 m a.s.l. (NHN). Both cores were opened, cleaned, photographed, described, and sampled in the laboratory. Descriptions of stratigraphic units followed the standard procedure given by Ad-hoc-AG Boden (2005) and Schrott

**TABLE 1** Overview of vibracore and Cone Penetration Testing/Hydraulic Profiling Tool (CPT/HPT) locations referred to in this study (a.s.l., above sea level, NHN).

Core ID (numerical order)	Northing (UTM/ETRS89 zone 32 N)	Easting	Elevation (m a.s.l.)	environment (recent)	coring type	Publication (original)
RUN 1	6035803.454	483335.661	0.29	tidal flat	vibracore	Hadler et al., 2018b
RUN 2A	6037157.700	483446.700	-0.66	tidal flat	push core	Hadler & Vött, 2016; Hadler et al., 2018b
RUN 3A	6037183.811	483454.012	-0.84	tidal flat	push core	Hadler & Vött, 2016; Hadler et al., 2018b
RUN 4A	6037187.891	483447.285	-0.73	tidal flat	push core	Hadler & Vött, 2016; Hadler et al., 2018b
RUN 6	6035493.239	481996.484	2.24	salt marsh	vibracore	Hadler et al., 2018b
RUN 6A	6035492.928	481995.224	2.27	salt marsh	vibracore	Hadler et al., 2018b
RUN 7A	6035393.431	482002.107	2.04	salt marsh	vibracore	Hadler et al., 2018b
RUN DP 7	6035392.762	482006.219	2.11	salt marsh	CPT/HPT sensing	this publication
RUN 17A	6035143.187	482081.801	1.80	salt marsh	vibracore	this publication
RUN 18A	6035124.205	482066.313	1.51	salt marsh	vibracore	this publication
RUN 18 DP	6035117.21	482063.066	1.67	salt marsh	CPT/HPT sensing	this publication
RUN 22A	6034794.641	481161.313	-0.99	tidal flat	vibracore	this publication
RUN 26A	6034660.102	481273.058	-0.69	tidal flat	vibracore	Hadler et al., 2018c
RUN 27A	6034630.784	481362.040	-0.65	tidal flat	vibracore	this publication

(2015) and comprised criteria like grain-size, sediment colour, carbonate content, macrofossil content, archaeological artefacts, and so forth. Results are supplemented with vibracore data previously published by Hadler and Vött (2016) and Hadler et al. (2018b, 2018c; Table 1).

### 3.2 | Palaeoenvironmental parameters (PEPs): Sedimentary, geochemical and microfaunal analyses

The cores underwent a broad multi-proxy analysis to characterize the palaeoenvironmental conditions of each stratigraphic unit and to identify different sedimentary facies (Hadler et al., 2018b).

Grain-size analyses were accomplished for 93 bulk samples from vibracore RUN 17A and RUN 18A using the sieving and pipette method after Köhn (1929). Samples were pre-treated with hydrogen peroxide (H<sub>2</sub>O<sub>2</sub>) and hydrochloric acid (HCl) to remove organic and carbonate components (Blume et al., 2011). Grain-size parameters were calculated using the GRADISTAT software (Blott & Pye, 2001).

The concentration of organic matter in each sample was determined as loss on ignition (LOI) by heating sediments for 2.5 h at 550°C (Blume et al., 2011). All LOI values were then corrected for structural water loss by subtracting 0.1% per 1% of clay (Barsch, 2000; Blume et al., 2011; Schmidt & Scheibner, 1988).

Magnetic susceptibility (MS) was measured *in situ* with a vertical resolution of 1 cm using a Bartington MS2 instrument and a MS2K surface sensor (Bartington Instruments Ltd, Witney, UK). MS can be used to identify palaeosols since soil formation may cause a magnetic enhancement of sediments by the formation of magnetite (Dearing et al., 1996; Evans & Heller, 2003). Although this mineral tends to be dissolved in waterlogged, anoxic environments (Evans & Heller, 2003; Goldberg & Macphail, 2006; Hanesch & Scholger, 2005), in sulphate-rich brackish and marine environments and waterlogged gleyic soils magnetotactic and sulphate-reducing bacteria may form the

ferrimagnetic iron sulphide greigite (Fe<sub>3</sub>S<sub>4</sub>) and thereby induce a relative magnetic enhancement of the soil (Heywood et al., 1990; Hilton, 1990; Mann et al., 1990; Stanjek et al., 1994; Wheeler et al., 1999). For the study area, MS values proved to be a reliable proxy for fossil soils (Hadler et al., 2018b).

Concentrations of up to 30 elements were measured by X-ray fluorescence (XRF) analyses at an average interval of 2 cm, using a portable Niton XL3t 900S GOLDD instrument (calibration mode SOIL; Thermo Fisher Scientific, Waltham, MA, USA). Due to different matrix effects (e.g., particle size, uniformity, surface geometry, moisture), geochemical analyses based on portable XRF analysis as well as scanner-based XRF analysis are considered semi-quantitative (Chagué-Goff et al., 2015, 2017; EPA, 2007), but represent an approved and accepted tool in palaeoenvironmental research (Judd et al., 2017). The acquired data was normalized through calculation of elemental ratios to avoid effects of moisture or sediment matrix (Croudace et al., 2006; Richter et al., 2006; Rothwell, 2015). For the study area, the zirconium/rubidium (Zr/Rb) ratio proved a suitable proxy for energetic conditions during sediment deposition (Hadler et al., 2018b). While Rb is mainly adsorbed on clay minerals, Zr is commonly associated with heavy minerals of coarser fractions (Kabata-Pendias, 2011; Hutton, 1977; Rothwell et al. 2006; Rothwell, 2015). The titanium/calcium (Ti/Ca) ratio is a common indicator for weathering since easily soluble calcium carbonate is leached during soil formation, while rather immobile Ti is relatively enriched (Fischer et al., 2012; Kabata-Pendias, 2011). Iron (Fe) and sulphur (S) are used as indicators for reducing conditions and/or soil formation processes as both elements are associated with mineral formation by microbial activity (Croudace et al., 2006; Kabata-Pendias, 2011; Schroeder & Brümmer, 1968). Iron also correlates well with clayey sediments, frequently enriched in marsh soils (Reineck, 1982).

Microfaunal analyses with a focus on foraminifera and ostracod assemblages were conducted for 19 sediment samples from core

TABLE 2 Radiocarbon and dendrochronological ages of samples from the tidal flats around Hallig Südfall

Sample ID (radiocarbon)	Depth (m b.s.)	Depth (m a.s.l.)	Description	Lab. No. (MAMS)	<sup>14</sup> C age (yr BP)	δ <sup>13</sup> C (ppm)	2σ max; min (cal BC/AD)	Publication (original)
RUN 2A/3 M2	0.81	-1.47	articulated mollusc, <i>Cerastoderma edule</i>	19780	926 ± 18	-1.4	1393–1640 cal AD	b
RUN 3A/4 PR	0.79	-1.63	unidentified plant remains	19781	2063 ± 22	-33.4	155 cal BC; 7 cal AD	c
RUN 3A/5 PR	0.86	-1.70	unidentified plant remains	19782	724 ± 18	-34.9	1269–1295 cal AD	b
RUN 6/13 PR*	2.83	-0.59	unidentified plant remains	19783	—	—	—	c
RUN 6/23 PR	6.38	-4.14	wood remain	19784	7008 ± 26	-30.0	5983; 5804 cal BC	c
RUN 6/25 M	6.62	-4.38	articulated mollusc, <i>Cerastoderma edule</i>	19785	3507 ± 21	-7.4	1509–1223 cal BC	c
RUN 7A/6 HK	0.86	1.18	Charcoal	19786	2030 ± 19	-29.6	92 cal BC; 57 cal AD	c
RUN 7A/10 PR	1.04	1.00	unidentified plant remains	19787	231 ± 18	-36.4	1641; 1950* cal AD	c
RUN 10A/5 PR	0.61	-1.31	unidentified plant remains	19788	12940 ± 40	-29.1	13677–13351 cal BC	c
RUN 17A M	2.12	-0.32	articulated mollusc, <i>Cerastoderma edule</i>	41273	914 ± 21	-0.1	1403–1645 cal AD	a
RUN 17A PR	2.20	-0.40	unidentified plant remains (bulk sample)	41274	3257 ± 22	-26.9	1609; 1451 cal BC	a
RUN 18A/10 M	2.11	-0.60	articulated mollusc, <i>Scrobicularia plana</i>	41275	1209 ± 21	-2.2	1142–1399 cal AD	a
RUN 18A PR	2.20	-0.69	unidentified plant remains	41276	-1317 ± 18	-24.9	—	a
RUN 26A/4 + PR	0.72	-1.41	unidentified plant remains	41277	3245 ± 25	-29.7	1600; 1439 cal BC	a
RUN 26A/5 PR	0.75	-1.44	unidentified plant remains	41278	2556 ± 24	-29.0	801–569 cal BC	a
RUN SPLINT 1	0.20	-0.90	Wood	20619	779 ± 15	-19.6	1226–1275 cal AD	b
Sample ID (radiocarbon)	Depth (m b.s.)	Depth (m a.s.l.)	Description	Lab. No. (KIA)	<sup>14</sup> C age (yr BP)	δ <sup>13</sup> C (ppm)	2σ max; min (cal BC/AD)	Publication (original)
Wooden beam A** (Schleusendrempel Nr. 1.1)	0.00	0.00	—	—	—	—	—	—
Wooden beam B**	0.00	—	recovered from tide gate	81,578	—	—	37 growth rings, insufficient for reliable synchronization	d
Wooden beam C**	0.00	—	recovered from tide gate	81,579	AD 1269	AD 1331	63 growth rings; no sapwood, felling c. after AD 1351	d

Note: b.s., below ground surface; a.s.l., above present sea level (NHN); Lab. No., laboratory number; MAMS, Curt-Engelhorn-Centre for Archaeometry, Mannheim; KIA, <sup>14</sup>C-Lab Kiel; DAI, Dendrochronological Laboratory, German Archaeological Institute, Berlin; 1σ max;min (cal BC/AD), calibrated ages, 1σ range; 2σ max;min (cal BC/AD), calibrated ages, 2σ range; ; ; there are several possible age intervals due to multiple intersections with the calibration curve. Calibration based on Calib 8.2 software with calibration curves IntCal20 for non-marine samples and Marine20 for marine samples (Heaton et al., 2020; Reimer et al., 2020). Reservoir correction (Delta R) for the German Wadden Sea, according to the marine database: Delta R-85±17 (Enters et al., 2021); \*, carbonate content insufficient for dating; \*\*, dating results provided by NordseeMuseum Husum. Original publication of dating results: a, this publication; b, Hadler and Vött (2016); c, Hadler et al. (2018b); d, Hadler et al. (2018a).

RUN 18A. Briefly, 15 mL of sediment were retrieved from selected facies type and split into three fractions,  $\geq 400 \mu\text{m}$ , 400 to  $> 200 \mu\text{m}$  and 200 to  $> 125 \mu\text{m}$  (see also Finkler et al., 2018). All samples were counted wet and, if possible, for total species amounts using a stereo microscope (Type Nikon SMZ 745 T). Samples with high numbers of individuals were split according to Scott and Hermelin (1993).

In all samples, foraminifera occur in significantly higher abundances than ostracods. Species identification is based on taxonomic descriptions and illustrations by Murray (1971) and Horton and Edwards (2006). The different ecological spectra were assessed based on Sen Gupta (1999), Scott et al. (2001) and Murray (2006) as well as local studies of recent assemblages (Lehmann, 2000; Müller-Navarra et al., 2016, 2017, 2019). The species *Elphidium williamsoni* and *Elphidium excavatum* are summarized as *Elphidium* spp.

Ostracod species and associated ecological spectra were identified using the descriptions in Athersuch et al. (1989) and Frenzel et al. (2010). Different species of *Leptocythere* (mainly *L. psammophila*) are summarized as *Leptocythere* spp., as it is difficult to distinguish juvenile individuals. Macrofossil remains were determined according to Willmann (1989).

### 3.3 | Dating approach

Six samples of organic material and biogenic carbonate were selected for carbon-14 ( $^{14}\text{C}$ ) accelerator mass spectrometry (AMS) dating (Table 2) to establish a chronostratigraphy for the Hallig Südfall geo-archive. Although plant remains, wood or charcoal prevent reservoir effects, articulated bivalves may provide better results for the study area, as other samples frequently appear to be reworked and/or displaced by tidal dynamics and/or storm surges. Articulated bivalves, however, are either preserved in living position or – if reworked – deposited close to their die-off. Conventional radiocarbon ages were calibrated using the software Calib 8.2 with calibration curves IntCal20 and Marine20 using a local reservoir correction of  $\Delta R = 85 \pm 17$  as reported by Enters et al. (2021). Although uncertainties remain, ages obtained from local reservoir correction are generally considered more reliable for this area than ages based on the mean global reservoir correction. Two samples (RUN 17A PR, RUN 18A PR) were excluded from interpretation, as they are most likely reworked or yield a modern age, respectively. Samples that produced age inversions were also excluded, as the local environmental dynamics (tides, waves, storms) make reworking of older material likely.

New dating results are supplemented by 11 recalibrated radiocarbon ages and two dendrochronological ages from Hadler et al. (2018b, 2018a). Archaeological age estimations of finds from the tidal flats also helped cross-checking radiometric ages (Kühn, 2016). All dating results are summarized in Table 2.

### 3.4 | Direct Push (DP)-based *in situ* Cone Penetration Testing (CPT) and Hydraulic Profiling Tool (HPT)

At coring site RUN 18A, DP-based sensing methods were applied (RUN DP 18) using a Geoprobe 540 MO mast mounted on an automotive drill-rig type Nordmeyer RS 0/2.3 (Nordmeyer SMAG,

Braunschweig, Germany) equipped with HPT (K8058 probe, Geoprobe, Salina, KS, USA) and CPT (NOVA probe, Geotech, Askim, Sweden). Separate soundings of CPT and HPT allowed *in situ* measurements of different stratigraphic parameters with 2 cm vertical resolution and sensing depths of up to 15 m b.s. and 18 m b.s., respectively. Compared to vibracoring, CPT and HPT sensing is considerably more time-efficient, and results remain unaffected by artificial compaction or loss of sediment (for further reading on methodological details, see Obrocki et al., 2020). Yet, as the data needs to be calibrated, a combined approach of CPT and HPT sensing and vibracore key sites significantly improves palaeogeographic reconstructions of a site (Hadler et al., 2020).

The HPT dataset comprises the EC, water injection pressure (Pinj) and the estimated hydraulic conductivity (est.K), generally reflecting variations in grain size (Geoprobe, 2015). High values of EC and Pinj indicate fine-grained (clay, silt), low values coarse-grained (sand, gravel) deposits. Low est.K values are associated with small grain sizes that impede the passage of water, while high values point to coarser deposits. In terms of grain size distributions, Pinj and est.K are considered more reliable, as EC also depends on groundwater chemistry and mineralogy (Fischer et al., 2016; Wunderlich et al., 2013).

The CPT dataset comprises the corrected tip resistance ( $q_t$ , tip resistance  $q_c$  corrected for pore pressure effects; Robertson, 1990) and corrected sleeve friction ( $f_t$ , sleeve friction  $f_s$  corrected for pore pressure effects; Robertson, 1990) as well as the pore pressure ( $u_2$ ). The values of  $q_t$  and  $f_t$  were used to calculate the normalized friction ratio (Fr) to assign specific soil behaviour types (SBTs; Robertson, 1990) to each facies type. Like HPT, CPT data reflects grain size variations, but also the *in situ* mechanical behaviour of the sediment depending on stress, stiffness, microfabric or mineralogy (Lunne et al., 2002; Robertson, 2009). Thus, results may differ from measured grain sizes. Soil classification charts (e.g., Begemann, 1965; Douglas & Olsen, 1981; Jefferies & Davies, 1993; Robertson, 1990, 2009) allow an automated stratigraphic interpretation of CPT data based on the *in situ* mechanical behaviour of a facies type. However, these charts reflect lithological rather than palaeoenvironmental issues and do also not consider HPT data.

As the visual inspection of both, CPT and HPT data shows a high correlation with facies and unit boundaries derived from vibracoring, this study requires a new approach in facies classification. We therefore apply multivariate LDA as statistical approach to combine vibracore data and CPT/HPT parameters and to automatically identify and differentiate between facies types.

### 3.5 | Multivariate linear discriminant analysis (LDA) of Direct Push (DP) data

LDA is a multivariate statistical method to test structures, that is, classified groups that were already assigned to a dataset. Multiple groups LDA is used to determine the potential of different metric variables (here: DP parameters) to discriminate between three or more given groups (in our case facies types). It requires a dataset with variables available for different objects (e.g., sediment samples) of known group membership. The calculation of one or more linear discriminant function then allows a classification of the dataset with maximum inter-

group variance relative to the intra-group variance (Bahrenberg et al., 2008; Backhaus et al., 2016).

The standard equation is  $y = a + b_1 * x_1 + b_2 * x_2 + \dots + b_n * x_n$ , where  $y$  is the discriminant score for each object,  $a$  is a constant,  $b_i$  are the discriminant coefficients and  $x_i$  the individual values of the discriminating variables (Backhaus et al., 2016).

After deriving one or more discriminant functions from the original (training) dataset, LDA can be used to best predict group membership (here: facies types) of new objects (here: sediment samples), that is, classify those objects based on experience from the training dataset. This approach was already successfully applied by Vött et al. (2002), who used geochemical parameters to assign sediment samples from vibracores to different sediment facies. For this study, LDA is applied to a DP dataset to automatically assign each measuring point of the DP sensors to a specific facies type, allowing an objective and automated interpretation of DP logs.

In a first step, vibracore stratigraphies were divided into facies types (groups A to G) according to available PEPs such as grain-size, sediment colour, geochemistry, macrofossil content, archaeological artefacts, and so forth. These groups were then manually assigned to the DP training dataset collected from the same site, considering effects of sediment compaction and loss of material in vibracores as well as distinct changes in the DP data. All DP data were linearly interpolated on a 1 cm depth scale using the 'linterp' function of the 'astrochron' R package (Meyers, 2014; R core Team, 2014).

Using the forward stepwise approach of the Statistica 10 software package (StatSoft, 2011), variables were integrated step-by-step into the discrimination model, starting with the most discriminating variable. Compared to the SBT classification by Robertson (1990), the approach of which is merely based on CPT data, our LDA approach integrated variables from both CPT (here: qt, ft, u2, Rf) and HPT (here: EC, Pinj, est.K) sensing. In a last step, the validity of the LDA model was tested by data reclassification and calculation of classification rates for the original as well as a new dataset (RUN DP 7). A classification matrix allows a quantitative evaluation of the actual quality of discrimination. The standardized coefficient indicates the proportion of each variable in discriminating between groups (StatSoft, 2011).

### 3.6 | Reflection seismic

Seismic data was obtained to allow a lateral extrapolation of facies identified from vibracoring and/or LDA-based classification of CPT/HPT data. The seismic dataset comprises two 48 m profiles (SEIS 40 and SEIS 41, see Figure 1) with 24 horizontal geophones each. A sledgehammer and metal bar were used to excite horizontally polarized shear-waves. Shots were performed every 2 m in between each pair of geophones in SH-polarization (perpendicular to the profile). Data was recorded by a Geometrix Geode seismograph with 8 kHz sampling frequency. The data was used for reflection seismic processing to obtain a zero offset seismic section. For data processing, the open-source software Seismic Unix (<https://github.com/JohnWStockwellJr/SeisUnix>) was used. Post-processing steps included (1) setting coordinates and offsets, (2) sorting for CMPs (common midpoints), (3) NMO-correction with a constant average velocity of  $75 \text{ m s}^{-1}$  (profile SEIS 40) and using a velocity gradient from  $50 \text{ m s}^{-1}$  at the surface increasing to  $100 \text{ m s}^{-1}$  at 6 m depth

(profile SEIS 41), that was estimated from Love-wave inversion (using the code of Wilken and Rabbel [2012]), (4) stacking traces of less than 4 m offset for each CMP, (5) trace balancing by the first quantile of a trace, (6) trapezoidal bandpass filter with 16, 24, 120 and 160 Hz corner frequencies, (7) spreading and damping time correction (exponent 1.5), and (8) time to depth conversion.

## 4 | RESULTS

### 4.1 | Palaeoenvironmental parameter (PEP) analyses of vibracores RUN 17A and RUN 18A

Based on sedimentary, geochemical and microfaunal PEPs, eight major units (groups A to G) were identified for both vibracores and assigned to specific sedimentary facies and subfacies (Figures 3, 4 and 5). Sedimentary facies are hereby defined as the primary characteristics of a unit, that is, the lithological, geochemical, or biological characteristics (Reineck & Singh, 1980). Subfacies generally reflect the same superior deposition conditions (e.g., a tidal flat) but significantly differ within some primary characteristics (e.g., grain size variability between tidal sand, mixed or mud flat) (Schäfer, 2020).

#### 4.1.1 | Unit A (recent lower to high salt marsh)

The unit consists of dark grey, locally rust-coloured sandy mud with several layers of fine sand in the upper part. Sediments show typical characteristics of wet soils. The Ti/Ca ratio and MS values are high but decrease towards the top, while LOI values increase. Foraminifera reach a maximum number of individuals and are dominated by hyaline species of tidal flat to low marsh environments like *Haynesina germanica*, *Ammonia beccarii* and *Elphidium* spp. (Horton et al., 1999; Horton & Edwards, 2006; Scheder et al., 2019). Ostracods mainly comprise *Pontocythere elongata* as well as *Leptocythere* spp. and *Semicytherura sella*, all associated with sandy substrate and a shallow water outer estuarine environment (salinity > 30 ‰; Athersuch et al., 1989; Frenzel et al., 2010). Unit A represents the recent lower to high salt marsh environment, strongly influenced by the sea, showing characteristic features of a hydromorphic soil such as reduction (only RUN 17A) and oxidation (WRB: gleysol, Ad-hoc-AG Boden, 2005). Due to the lower topography, site RUN 18A is mostly unaffected by oxidation. Towards the top, geochemical and microfaunal proxies show that weathering and soil formation are suspended by frequent flood-related input of fresh marine sediments from the nearby tidal-flats (distance c. 20 m). Summarizing, unit A has the typical characteristics of a marsh facies. It is further classified as subfacies 'lower to high salt marsh that developed from a wave-dominated tidal sand flat'.

#### 4.1.2 | Unit B (fossil lower salt marsh)

The unit consists of compact, greenish grey clayey mud with strong features of both oxidation and reduction. A low Zr/Rb ratio indicates sedimentation under rather quiescent conditions. An increased Ti/Ca ratio attests to intense weathering. MS values are slightly



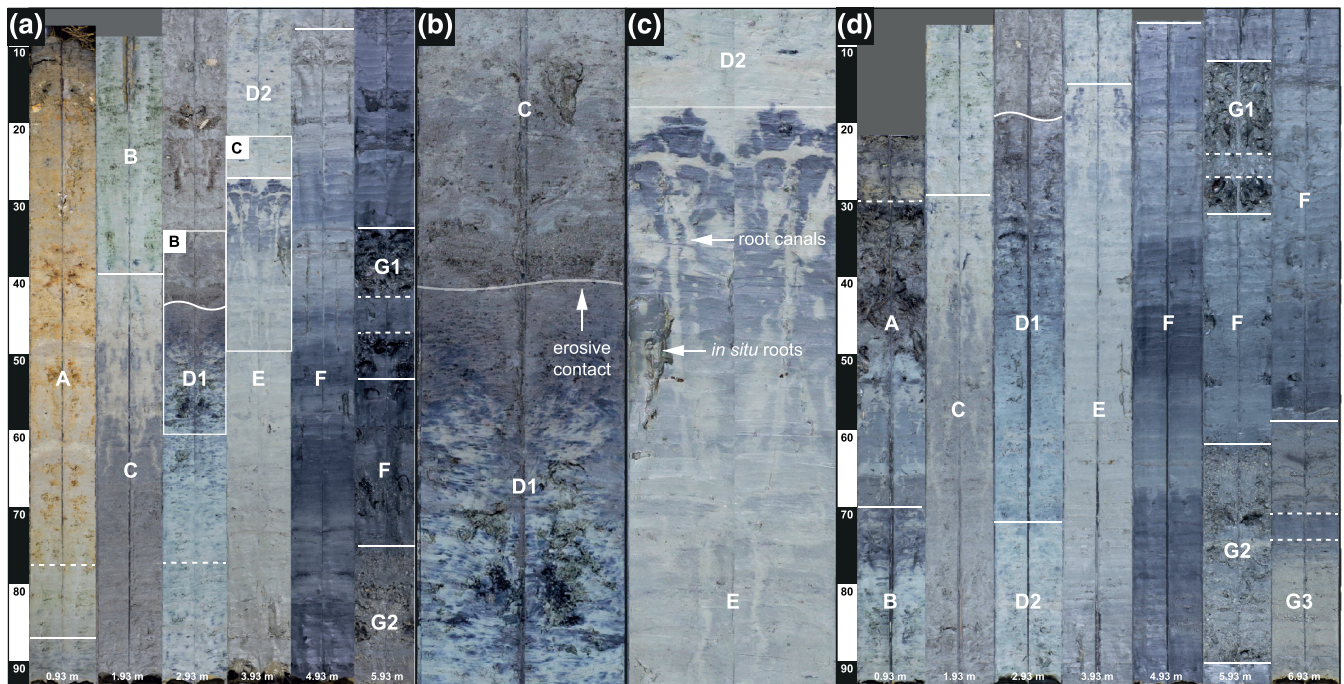


**FIGURE 3** Vibracore stratigraphies of RUN 17A (a) and RUN 18A (d). In both cores, a distinct erosive contact (b) marks the sudden transition from a marshland (D1) to tidal flat (C) environment, while the onset of early marsh formation is marked by a distinct mottling (c). Photographs: T. Willershäuser, 2016 [Color figure can be viewed at [wileyonlinelibrary.com](http://wileyonlinelibrary.com)]

increased, while LOI and S decrease towards the top. High Fe values correlate with a high clay content. The pH-value remains stable around pH 8.

Plant macro-remains comprise some roots and abundant *Juncus* sp. seeds that point to wet but clearly terrestrial conditions (Schoch et al., 1988). Foraminifera are few but significantly increase in number towards the very top. Hyaline species of tidal flat to low marsh environments like *Haynesina germanica*, *Ammonia beccarii* and *Elphidium* spp. are predominant but agglutinated species typical of middle and even high marsh environments like *Entzia macrescens* and *Trochammina inflata* also occur, the latter especially towards the top (Gehrels & Newman, 2004; Horton & Edwards, 2006; Horton et al., 1999; Müller-Navarra, 2018; Murray, 2006). Apart from a single valve of *Leptocythere* sp., sediments are void of ostracods.

Unit B reflects the transition from a quiescent semi-terrestrial to a terrestrial environment, that is, from the pioneer zone, still frequently flooded, to the lower salt marsh where constant sedimentation raises the surface within the range of MHW (Bartholdy, 1997, 2012). Although sediment colour still indicates reducing conditions, aeration seems enough for the decay of organic matter and oxidation of sulphides to sulphuric acid that is washed out from the soil (Scheffer & Schachtschabel, 2018). Summarizing, unit B also has typical features of a marsh facies classified as subfacies 'fossil lower salt marsh developed from tidal mixed flat'. Covered by younger marsh deposits of unit A, it represents a fossil soil horizon called 'Dwogmarsch' (LLUR, 2012; Müller, 1958).

#### 4.1.3 | Unit C (fossil tidal mud flat)

Sediments consist of very poorly sorted grey, sandy mud with a distinct blackish mottling at the top. The layer shows a sharp (erosive)

contact towards underlying unit D1 (Figure 3b) but gradually changes into overlying unit B. A notable sand content and highest Zr/Rb values indicate increased energetic conditions, while low Ti/Ca and MS values point to rather unweathered sediments with increased content of diamagnetic quartz sand (Dearing, 1999). Low Fe values reflect the overall low clay content (Reineck, 1982). At the very base, sediments contain abundant calcium sulphate minerals (gypsum, anhydrite) that are known to precipitate where calcareous seawater is mixed with sulphuric acid (e.g., from decay of organic matter in [semi-]terrestrial environments; Hecht, 1933). An increased basal S content may reflect a relative enrichment by microbial reduction of sea water sulphides (Schroeder & Brümmer, 1968), decreasing towards the top.

The macrofauna includes articulated specimens of *Cerastoderma* sp. (cockle) and *Scrobicularia plana* (peppery furrow clam), individuals of *Peringia ulvae* (mud snail) and *Retusa obtusa* (Arctic barrel-bubble) as well as jaws of *Hediste* sp. (ragworm), all typical of outer tidal (mud) flat environments (Reineck, 1982; Willmann, 1989). Few oribatid mites indicate nearby (semi-)terrestrial conditions, that is, a saltmarsh environment (Polderman, 1974).

Foraminifera mainly comprise the tidal flat species *Haynesina germanica*, *Ammonia beccarii* and *Elphidium* spp. *Ammonia beccarii* even reaches its highest abundance. Low numbers of *E. macrescens* suggest a near-coast environment (Scheder et al., 2019). In the lower part, ostracods are dominated by *Leptocythere* spp. that is frequently found in mud flat environments (Penney, 1987). Towards the top, it is gradually replaced by the euryhaline *Cyprideis torosa*. Prevailing irregular sieve pores and the absence of nodding in randomly checked individuals of *Cyprideis torosa* point to salinities > 7 ‰ (Frenzel et al., 2012, 2017; Rosenfeld & Vesper, 1976). Although generally considered as index fossil for brackish conditions (Athensuch et al., 1989; Frenzel et al., 2010; Pint et al., 2012; Rosenfeld & Vesper, 1976), the strong

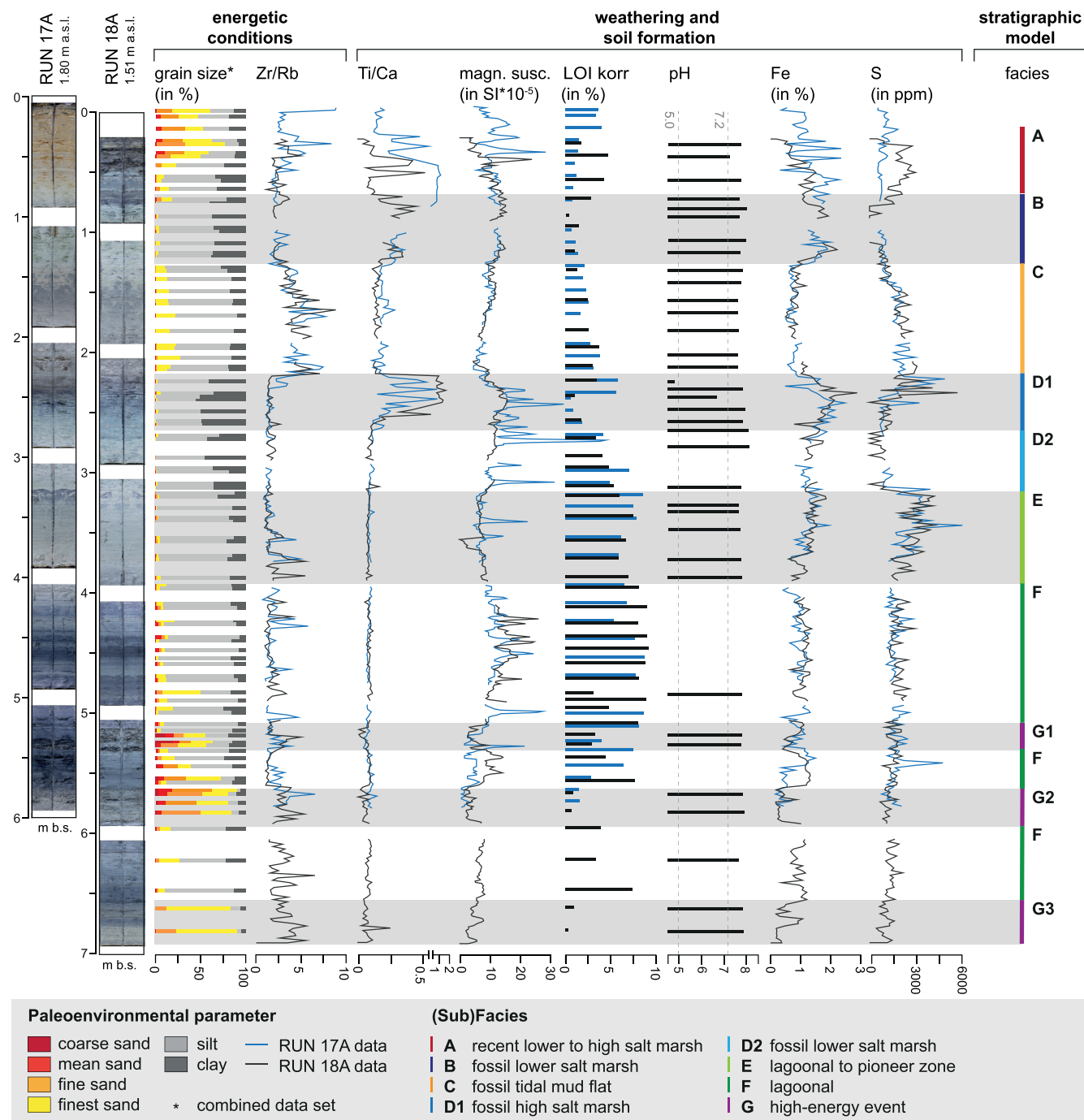


**FIGURE 4** Palaeoenvironmental parameter (PEP) analyses allow the identification of different facies for vibracores RUN 17A and RUN 18A that provide a stratigraphic model for Hallig Südfal [Color figure can be viewed at wileyonlinelibrary.com]

increase and finally monospecific occurrence of *Cyprideis torosa* and simultaneous decrease of *Leptocythere* spp. rather reflect a significant increase in environmental stress (e.g., tidal influence, salinity, and temperature changes; Penney, 1987).

Unit C reflects a marine tidal mud flat environment with initially increased flow or wave dynamic that abruptly established on top of the underlying unit D1. Proxies then indicate a gradual shift towards calmer but ecologically variable conditions of a semi-terrestrial pioneer zone environment. Unit C therefore reflects a tidal flat facies and is further classified as subfacies ‘tidal mud flat’.

#### 4.1.4 | Unit D1 (fossil high salt marsh)

The unit comprises compact, bluish grey clayey mud with strong hydromorphic features. It shows a gradual lower and a sharp, erosive upper contact. A high clay content, lowest Zr/Rb and highest Ti/Ca values indicate low-energy depositional conditions and intense weathering, respectively. MS values are high but decline in the uppermost part. LOI gradually decreases upward but is strongly enriched at the very top. The S values are low but increase towards the top. High Fe values correlate with the high clay content. The pH value drops to a minimum of 4.8 (Figure 4).

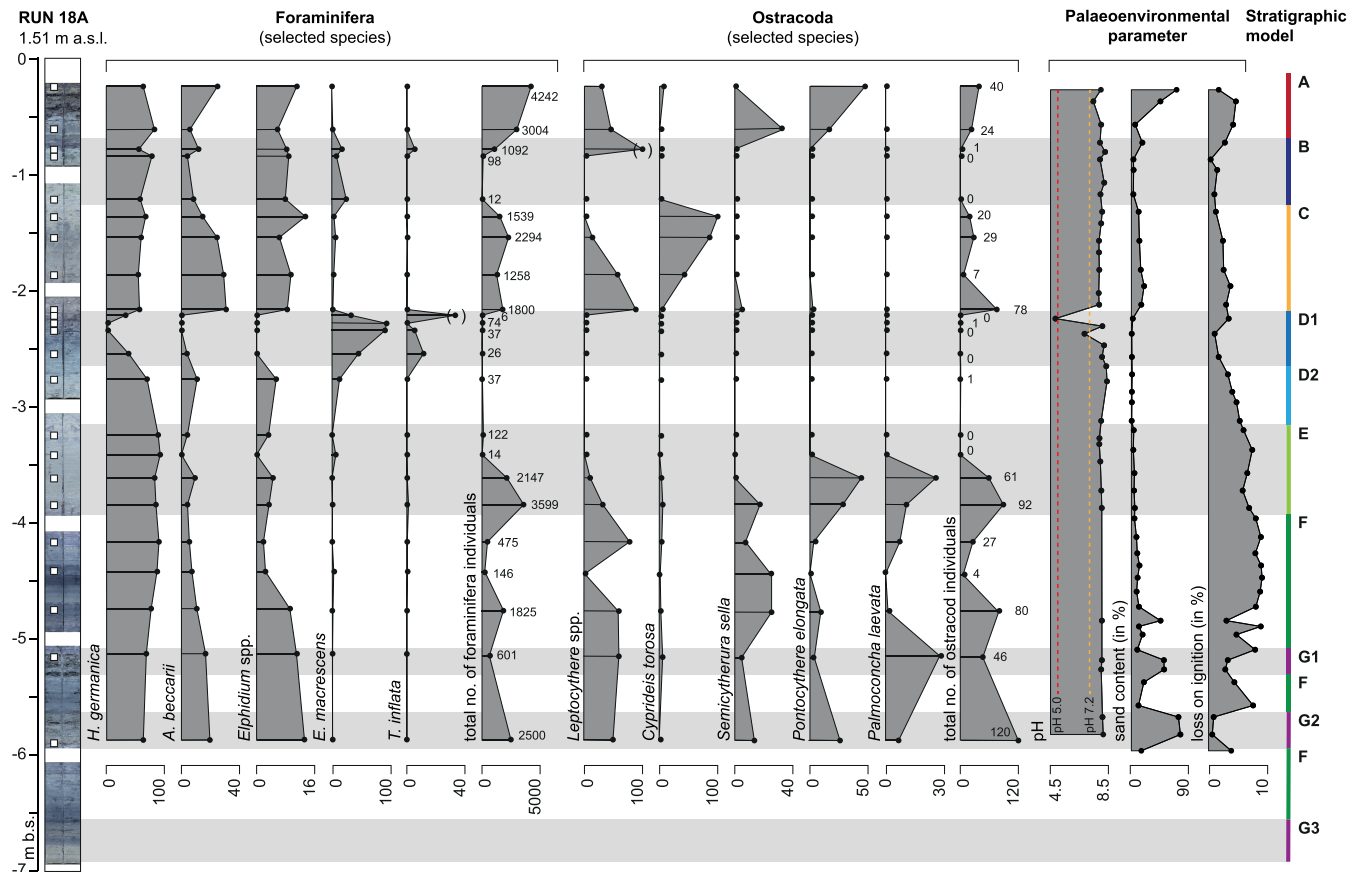


FIGURE 5 Microfaunal results of vibracore RUN 18A [Color figure can be viewed at [wileyonlinelibrary.com](http://wileyonlinelibrary.com)]

Macro-remains comprise abundant *Juncus* sp. seeds, *Phragmites* sp. roots and a single oribatid mite, all indicative of a terrestrial environment with wet conditions (Schoch et al., 1988). Foraminifera are few and agglutinated species typical of middle to high marsh environments like *E. macrescens* and *T. inflata* dominate (Figure 5), while hyaline species are nearly absent (Gehrels & Newman, 2004; Horton & Edwards, 2006; Horton et al., 1999; Müller-Navarra, 2018; Murray, 2006). Corresponding to terrestrial conditions, sediments are void of ostracods as they do not survive prolonged periods of subaerial exposure (Penney, 1987). Apart from environmental changes (e.g., decreasing saltwater influence, terrestrial conditions), the generally low abundance of microfossils may also result from post-depositional dissolution of calcareous tests due to the decay of organic matter and/or acidic conditions (Berkeley et al., 2007; Edwards & Horton, 2000).

In total, unit D1 reflects a high salt marsh environment where ongoing sedimentation of fine-grained, organic-rich sediments raise the ground level above MHW, intensifying desalinization and soil aeration (Bartholdy, 1997, 2012). Subsequent oxidation of (Fe-)sulphides and the decay of organic matter produce Fe-oxides, sulphuric and carbonic acid causing a rapid decalcification and acidification of the sediment (Scheffer & Schachtschabel, 2018). Unit D1 is therefore associated with a marsh facies at the end of the marsh succession and classified as subfacies 'fossil high salt marsh developed from a lagoonal environment'. Covered by younger tidal flat deposits of unit C, it represents another fossil soil horizon called 'Dwogmarsch' (LLUR, 2012; Müller, 1958).

#### 4.1.5 | Unit D2 (fossil lower salt marsh)

The unit comprises of homogeneous mud of light grey colour indicating a reductive environment. The unit shows gradual lower and upper boundaries. An increasing clay content and low Zr/Rb ratio point to quiescent sedimentation conditions. The Ti/Ca values are low, revealing little weathering. As LOI gradually decreases, S is significantly reduced and the pH-value remains stable around pH 8, sediments still seem to be affected by initial soil formation processes (aeration, decay of organic matter, oxidation of sulphides; Scheffer & Schachtschabel, 2018). Similar to unit D1, thick roots penetrate the deposit and the microfaunal abundance is low. Foraminifera comprise only few individuals of *Haynesina germanica*, accompanied by *Ammonia beccarii* and *Elphidium* spp. and some agglutinated species like *E. macrescens*. Ostracods are nearly absent.

While unit D1 represents a high salt marsh, unit D2 rather reflects semi-terrestrial conditions of a frequently flooded lower salt marsh environment (cf. unit B), where constant siltation raises the ground surface to some decimetres below MHW. This induces environmental stress by high fluctuations in salinity and temperature during tides and/or seasons (Beetink & Rozema, 1993; Reineck, 1982) as well as initial soil formation processes (Scheffer & Schachtschabel, 2018). Summarizing, unit D1 also reflects a marsh facies but is classified as subfacies 'lower salt marsh developed from lagoonal environment'.

#### 4.1.6 | Unit E (lagoon to pioneer zone)

Sediments consist of rather soft, light grey mud with a distinct blackish mottling at the upper boundary (cf. Figure 3c). Upwards decreasing Zr/Rb and generally low Ti/Ca values show quiescent sedimentation unaffected by weathering. LOI and S gradually increase upward while pH remains stable around pH 8. Increased Fe values go along with the increased clay content.

Thick roots penetrate the deposit through well visible oxidized root canals. In the lower part, foraminifera are mainly dominated by *Haynesina germanica* with minor occurrences of *Ammonia beccarii* and *Elphidium* spp., all decreasing towards the top. Outer estuarine species with inverse trends dominate the ostracod assemblage. While *Leptocythere* spp. and *Semicytherura sella* decline, *Palmoconcha laevata* and the euhaline *Pontocythere elongata* (> 30 %; Frenzel et al., 2010) increase in numbers (Figure 5). All ostracods entirely disappear upwards, indicating a significant environmental shift within the unit.

To sum up, unit E reflects a distinct shift from a subtidal marine shallow water lagoonal environment to intertidal pioneer zone conditions, characterized by increased salinity or salinity fluctuations and accumulation of organic-rich mud (Reineck, 1982). Microbial reduction of sea water sulphides is known to significantly enrich S in freshly deposited muds (Schroeder & Brümmer, 1968). The distinct mottling along the upper boundary indicates the development of a characteristic monosulphide and disulphide zonation (Reineck, 1982). While foraminifera are present, ostracods are missing in the pioneer zone (Scheder et al., 2019). Unit E is therefore associated with a lagoonal to semi-terrestrial facies and further classified as subfacies 'shallow lagoon to pioneer zone'.

#### 4.1.7 | Unit F (brackish-marine lagoon)

The unit comprises very poorly sorted dark grey to almost black sandy mud, indicating a reductive environment. Thin layers of sand and fluctuating Zr/Rb values indicate short-term changes of energetic conditions. Low Ti/Ca values indicate negligible weathering effects. Reductive conditions and highest LOI values likely favour the magnetic enhancement of sediments by bacterial formation of ferrimagnetic iron sulphides (e.g., Fe<sub>3</sub>S<sub>4</sub>; Hadler et al., 2018b; Mann et al., 1990; Stanjek et al., 1994).

Foraminifera occur in average abundance with a dominance of *Haynesina germanica*, accompanied by few specimens of *Ammonia beccarii* and *Elphidium* sp. Ostracods occur at varying abundances and mostly comprise *Leptocythere* spp. but also *Semicytherura sella*, *Palmoconcha laevata* and *Pontocythere elongata*, the latter two increasing upward.

Unit F thus reflects a subtidal brackish-marine shallow water lagoonal environment, mostly sheltered from wave dynamics and/or currents and with predominantly reducing conditions. Summarizing, unit F is associated with a lagoonal facies and further classified as subfacies 'shallow lagoon with reductive conditions'.

#### 4.1.8 | Unit G (high-energy deposit)

The unit comprises three sedimentary layers that were found intersecting unit F sediments. The blackish to dark grey and very poorly

sorted layers consist of shell debris (G3), shell debris in a sandy matrix (G2) and predominantly sand (G1). Increased Zr/Rb values reflect increased energetic conditions. The Ti/Ca ratio, MS and LOI all show low values. The Fe values also decrease as the clay content declines.

The shell debris mainly comprises abundant fragments and single valves of *Cerastoderma* sp. and *Mytilus edulis* as well as *Peringia ulvae*. The foraminiferal assemblage strongly resembles unit F. *Leptocythere* sp. dominates the ostracod assemblage, accompanied by *Pontocythere elongata* or *Palmoconcha laevata* and few individuals of *Semicytherura sella*.

Unit G reflects high-energy brackish to marine conditions that repeatedly affect the lagoonal unit F environment, for example, storm events or short-lived tidal inlets. Thus, unit G is associated with a lagoonal facies but further classified as subfacies 'lagoon under temporary high-energy influence'.

In a summary view, the stratigraphic records from vibracores RUN 17A and RUN 18A comprise eight characteristic units, each of which is associated with a specific sedimentary (sub)facies. In the following, we will therefore only use the terms 'facies' and 'subfacies', as they reflect the characteristic depositional conditions of a certain environment.

As emphasized by Walther (1894), vertical sequences of genetically related facies result from successions of laterally juxtaposed depositional environments. The Hallig Südfall stratigraphy shows facies sequences typical of a succession from lagoonal to terrestrial (F-[G]-E-D2-D1) and tidal flat to terrestrial (C-B-A) environment, respectively. The lower facies sequence documents a gradual development from a sheltered brackish to marine shallow-water lagoonal environment (F, E) towards a first phase of salt marsh formation (D2, D1), that is, towards a terrestrial environment. The upper facies sequence shows that constant siltation within a tidal flat environment (C) subsequently leads to a second phase of salt marsh formation (B). Although terrestrial conditions continue, a third phase of salt marsh development (A) indicates an increased influence of tidal dynamics. This stratigraphy fits well to the generalized sequence of salt marsh development after Beeftink and Rozema (1993).

The marsh facies itself is further classified into subfacies A, B, D1 and D2 as they show major difference in the original depositional environment. The muddy subfacies D1 and D2 developed in a low-energy environment, while the sandier subfacies A and B each formed under increased wave or current dynamics. The sequence of subfacies E, D2 and D1 reflects the gradual formation of a lower (D1) to high salt marsh (D2) from brackish-marine lagoonal conditions, while the sequence of (sub)facies C, B and A reflects the development of a lower salt marsh (B) from a tidal mud flat environment (C), succeeded by a second phase of a rather wave-dominated lower to high salt marsh formation (A).

Similar stratigraphic sequences were found from vibracores RUN 6, RUN 6A and RUN 7A (Figure 1b; Hadler et al., 2018b), some 300 m north of the study site. Here, a thick layer of shell debris marks the additional occurrence of subfacies G close to or at the present-day ground surface. Correlating subfacies were also found in the tidal flats southwest of Hallig Südfall at vibracoring sites RUN 22A, RUN 26A (Hadler et al., 2018c) and RUN 27A and to the northeast of Südfall at vibracore site RUN 1 and push-core sites RUN 2A, RUN 3A and RUN 4A (Figure 1a; Hadler & Vött, 2016; Hadler et al., 2018b). Due to intense erosion, their stratigraphy merely comprises the lower

subfacies D1 to G, while the top subfacies A to C are missing. Instead, the upper part of these vibracores partly consists of recent tidal sand flat deposits. The latter are categorized as subfacies H 'tidal sand flat'.

A striking observation in the local stratigraphy of Hallig Süfall is the direct succession of the high marsh subfacies D2 and the tidal flat subfacies C (e.g., RUN 17A; Figure 3b). The respective sedimentary units are separated by a distinct erosive contact that indicates a hiatus in the local stratigraphic record and/or a drastic environmental change within the coastal environment of North Frisia.

## 4.2 | High-resolution Direct Push (DP) stratigraphies

CPT and HPT data were collected at the coring sites to test their applicability for detection and subsequent mapping of the facies that were classified on the base of sedimentological and PEP data. At the time of DP sensing, the local ground-water level was about 0.35 m b.s. at site RUN DP 18 and about 1.55 m b.s. at site RUN DP 7.

By visual comparison alone, the RUN DP 18 dataset reflects the predefined subfacies already quite well (Figure 6). This is especially true for the fossil (high) salt marsh subfacies B and D1 that are marked by peaks in the corrected sleeve friction  $f_t$  and pore pressure  $u_2$  both reflecting the stiff character, upward increasing clay content and thus reduced permeability of the encountered

sediments. The latter also results in a significantly increased average corrected HPT pressure  $P_{inj}$  and a minimum hydraulic conductivity  $est.K$ . In both subfacies, B and D1, the EC value is uncorrelated with the average corrected HPT pressure  $P_{inj}$  and hydraulic conductivity  $est.K$ , indicating the influence of pore water chemistry rather than grain size. The erosive contacts that mark the rapid environmental changes succeeding the fossil marsh environments are perfectly discernible from a strong decline in pore pressure  $u_2$  at the upper boundaries of the sedimentary units associated with subfacies D1 to C and subfacies B to A.

Less consolidated lower marsh deposits (lower subfacies B, subfacies D2) reveal a decreased pore pressure  $u_2$  but high friction ratio  $R_f$ . A decrease of the latter marks the gradual transition from the pioneer zone to salt marsh environments (upper subfacies E to D2, lower to upper subfacies B). A significantly increased corrected tip resistance  $q_t$  was only found for the well consolidated upper salt marsh subfacies D1. A distinct peak in the corrected tip resistance  $q_t$  at c. 0.8 m b.s. is most likely due to subsurface coastal protection works (fascines).

Since recent marsh deposits (subfacies A) are significantly coarser and less consolidated, the pore pressure  $u_2$  as well as average corrected HPT pressure  $P_{inj}$  and hydraulic conductivity  $est.K$  show inverse trends. EC values are low, but a distinct increase towards the ground surface attests to the influence of frequent marine flooding during high tides or by storm surges.

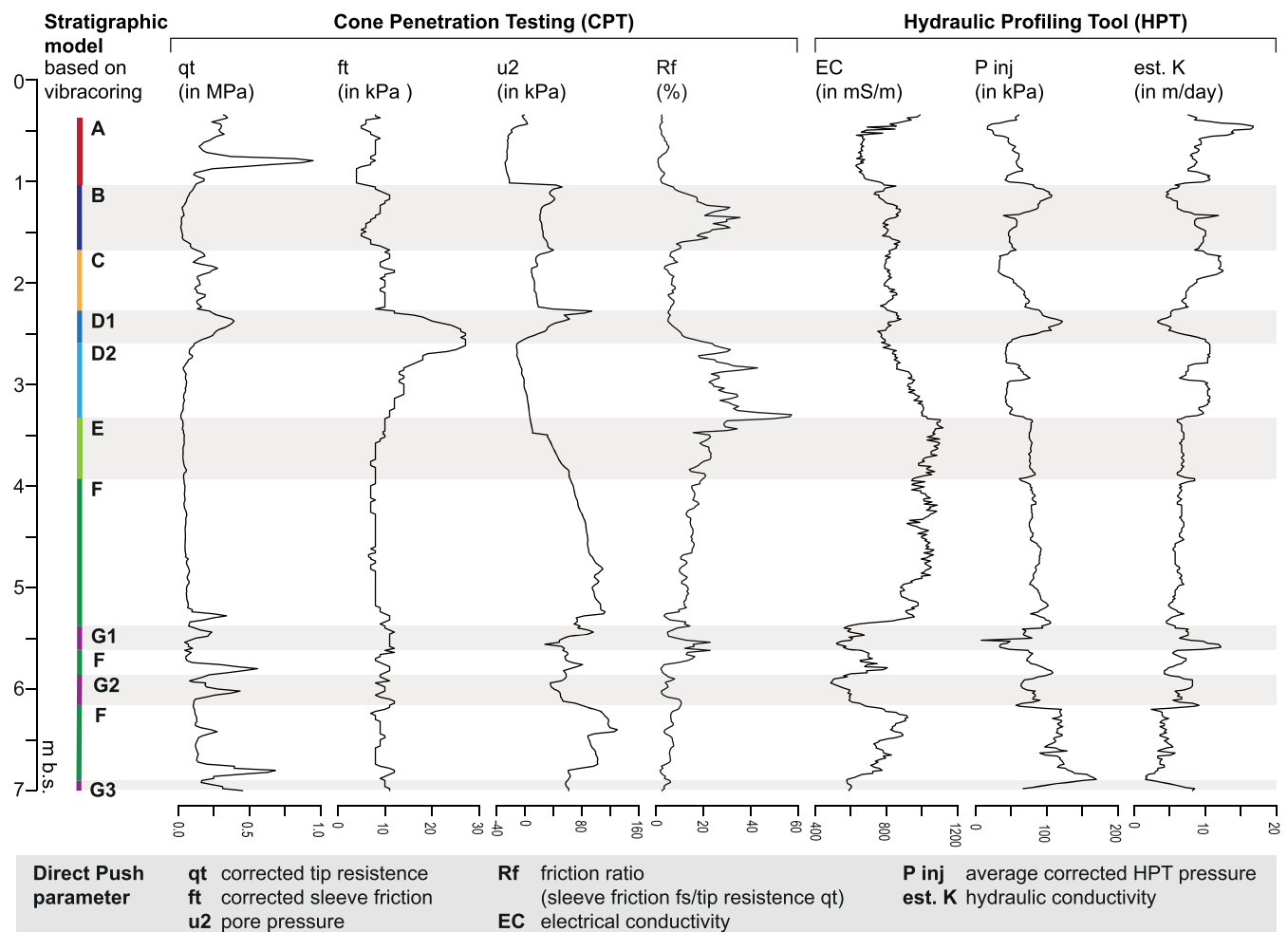


**FIGURE 6** Direct Push (DP) results for site RUN DP 18. Cone Penetration Testing (CPT) and the Hydraulic Profiling Tool (HPT) logs correspond with the stratigraphic model obtained by vibracoring and palaeoenvironmental parameter (PEP) analyses [Color figure can be viewed at [wileyonlinelibrary.com](http://wileyonlinelibrary.com)]

In-between subfacies B and D1, subfacies C shows a constant mean corrected tip resistance  $q_t$ , corrected sleeve friction  $f_t$  and pore pressure  $u_2$  that fit the softer and less cohesive sandy mud. Although grain size analyses rather attest to a fining upward within the associated sedimentary unit, the average corrected HPT pressure  $P_{inj}$  and hydraulic conductivity  $est.K$  show contradicting trends. This may be due to the increasingly brittle texture of the sediment. The EC is again uncorrelated with the average corrected HPT pressure  $P_{inj}$  and hydraulic conductivity  $est.K$ , indicating pore water influence.

Down to the level of mean low water (MLW, -1.69 m a.s.l.; BSH, 2020a), EC values rather seem to reflect pore water chemistry than grain size changes, while EC data below MLW correlates again with the grain size dependent average corrected HPT pressure  $P_{inj}$  and hydraulic conductivity  $est.K$ . EC values of subfacies D1 and D2 are clearly decreasing although the clay content increases. As the transition from subfacies E to D2 coincides with the level of MLW, sediments may also be affected by desalinization.

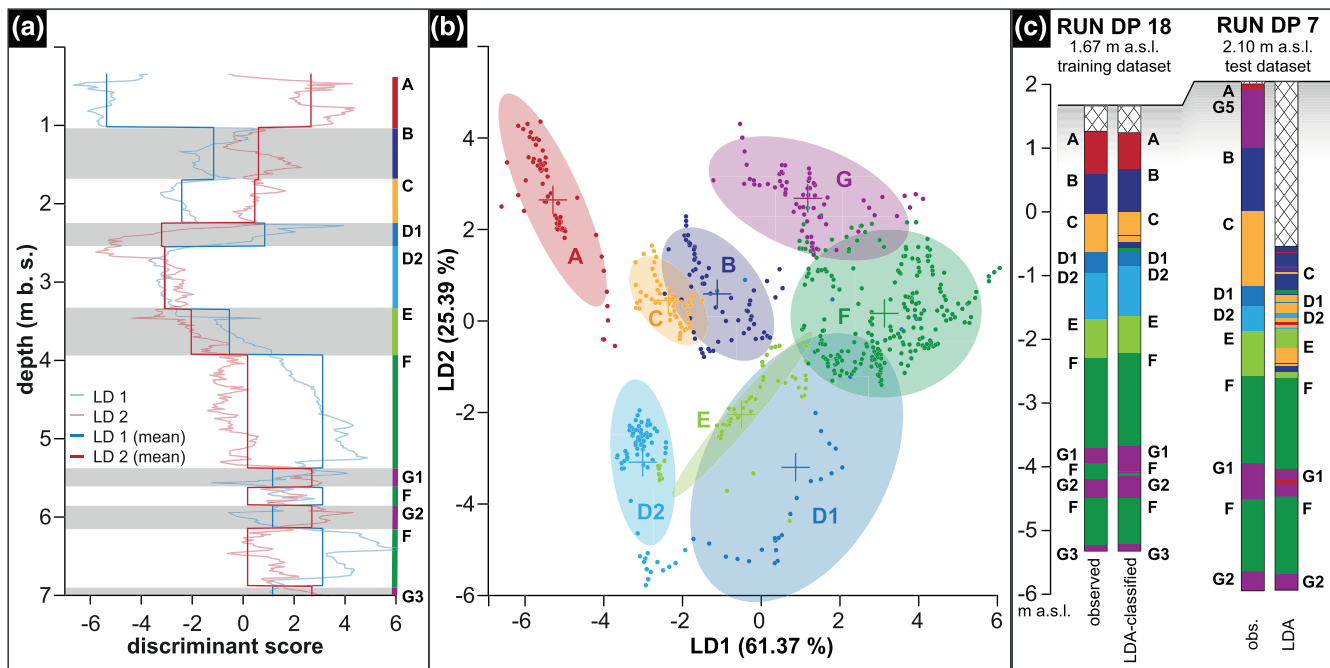
The soft and fine-grained sediments of subfacies E and F are well reflected by a low corrected tip resistance  $q_t$  and corrected sleeve friction  $f_t$ . An increase of the corrected sleeve friction  $f_t$  can only be found towards the top of subfacies E, as sediments become more

cohesive with the transition towards subfacies D1. The pore pressure  $u_2$  show a gradual downward increase.

The homogeneous fine-grained character of both facies becomes also evident from a stable average corrected HPT pressure  $P_{inj}$  and hydraulic conductivity  $est.K$ . EC values reach a maximum and correlate well with the average corrected HPT pressure  $P_{inj}$  and hydraulic conductivity  $est.K$ , attesting the EC to be grain size dependent. As subfacies E and F lie below MLW, significant changes in porewater chemistry can be neglected. This is also true for subfacies G, where the EC declines because of an increased grain size that also causes a slight increase in the corrected sleeve friction  $f_t$ . Subfacies G is further marked by significant increases in the corrected tip resistance  $q_t$  and simultaneous decreases in the pore pressure  $u_2$  that also fit the coarse-grained character of these shell debris and sand layers. A high water permeability is evident from a low average corrected HPT pressure  $P_{inj}$  but high hydraulic conductivity  $est.K$ .

### 4.3 | Multivariate linear discriminant analysis (LDA)

LDA was used to verify whether DP CPT and HPT data allow a discrimination between subfacies assigned during PEP analysis. The



#### Linear discriminant analysis of RUN DP 18

##### Variables (CPT):

corrected sleeve friction  $f_t$  (MPa)  
 corrected tip resistance  $q_t$  (MPa)  
 pore pressure  $u_2$  (MPa)  
 friction ratio  $R_f$  ( $[f_t/q_t] \cdot 100$  %)

##### Variables (HPT):

electrical conductivity EC (mS/m)  
 avg. corrected HPT pressure  $P_{inj}$  (kPa)  
 hydraulic conductivity  $est. K$  (m/day)

##### Proportion of trace:

LD1: 0.6137 LD3: 0.0938  
 LD2: 0.2539 LD4-7: 0.0395

##### Reclassification rates:

A: 94.12 % D2: 96.25 %  
 B: 95.52 % E: 96.55 %  
 C: 85.45 % F: 91.32 %  
 D1: 76.67 % G: 96.97 %  
 avg. RUN DP 18: 92.49 %

##### Discriminant potential of variables:

$u_2 > f_t > EC > q_t > R_f > est. K > P_{inj}$   
 n: 666  
 Wilks' lambda:  $6.45 \cdot 10^{-3}$

##### Classification rates for RUN DP 7:

A: - D2: 25.64 %  
 B: - E: 41.89 %  
 C: 6.25 % F: 98.79 %  
 D1: 9.68 % G: 66.67 %  
 avg. RUN DP 7: 64.88 %

**FIGURE 7** Linear discriminant analysis of RUN DP 18. The stratigraphic model obtained from vibracoring and palaeoenvironmental parameter (PEP) is used to set stratigraphic boundaries within the Direct Push (DP) dataset (a). Mean discriminant scores for LD 1 and LD 2 show the potential of each function to discriminate between the predefined subfacies. LD 1 separates best between terrestrial recent marsh (A1) and anoxic lagoonal (F) conditions, while LD 2 discriminates best between high-energy (G) and (semi)terrestrial (D) conditions. A scatter plot of LD 1 and LD 2 illustrates the high potential of both discriminant functions to differentiate between (sub)facies (b). Classification rates for RUN DP 7 show the large potential but also limitations of the RUN DP 18 training dataset (c) [Color figure can be viewed at wileyonlinelibrary.com]

training dataset for core RUN 18A contained 666 cases in eight different groups (subfacies A–G). Stepwise forward LDA resulted in seven discriminant functions (LD) where LD 1 to LD 3 describe 96.14% of the dataset's intergroup variance (Figure 7). LD 4 to LD 7 can thus be neglected.

Plotted against depth, mean discriminant scores (DSs) from LD 1 and LD 2 already allow a clear differentiation between subfacies (Figure 7a). LD 1 (eigenvalue 61.37%) differentiates especially between recent terrestrial (subfacies A, mean DS  $-5.35$ ) and lagoonal (subfacies F, mean DS  $3.10$ ) conditions but also separates the upper marsh formation complex of subfacies B and C (mean DS  $-1.16$  and  $-2.41$ , respectively). LD 2 (eigenvalue 25.39%) mostly differentiates the lower marsh formation complex of subfacies sequence D1, D2 and E (mean DS  $-3.19$ ,  $-3.08$  and  $-2.04$ , respectively) from the recent salt marsh and high-energy deposits (subfacies A and G, mean DS  $2.64$  and  $2.68$ , respectively).

A scatter plot of the individual discriminant scores from LD 1 (eigenvalue 61.37%) and LD 2 (eigenvalue 25.39%) further emphasizes the potential of the DP dataset for discriminating between (sub) facies (Figure 7b). Some overlaps occur but LD 1 and LD 2 clearly separate between facies types.

Classification rates were calculated by comparing the given groups of RUN DP 18 with LDA reclassification results (Figure 7c). The reclassification rate ranges from 76.67% (facies type D1) to 96.97% (subfacies G) and averages at 92.49%. To evaluate the performance of LDA-based DP sensing data classification, the discriminant functions obtained from the RUN DP 18 training dataset were applied to the test dataset RUN DP 7 (Figure 7c), located some 300 m north of RUN DP 18 close to vibracoring sites RUN 6/6A and RUN 7A. Measurements start at  $-0.5$  m a.s.l. creating a test dataset of 541 cases comprising subfacies C to G. Classification rates were equally calculated from comparison of vibracore-based groups assignments with the LDA-based classification and range from 6.25% (subfacies C) to 98.79% (subfacies F).

#### 4.4 | Seismic measurements

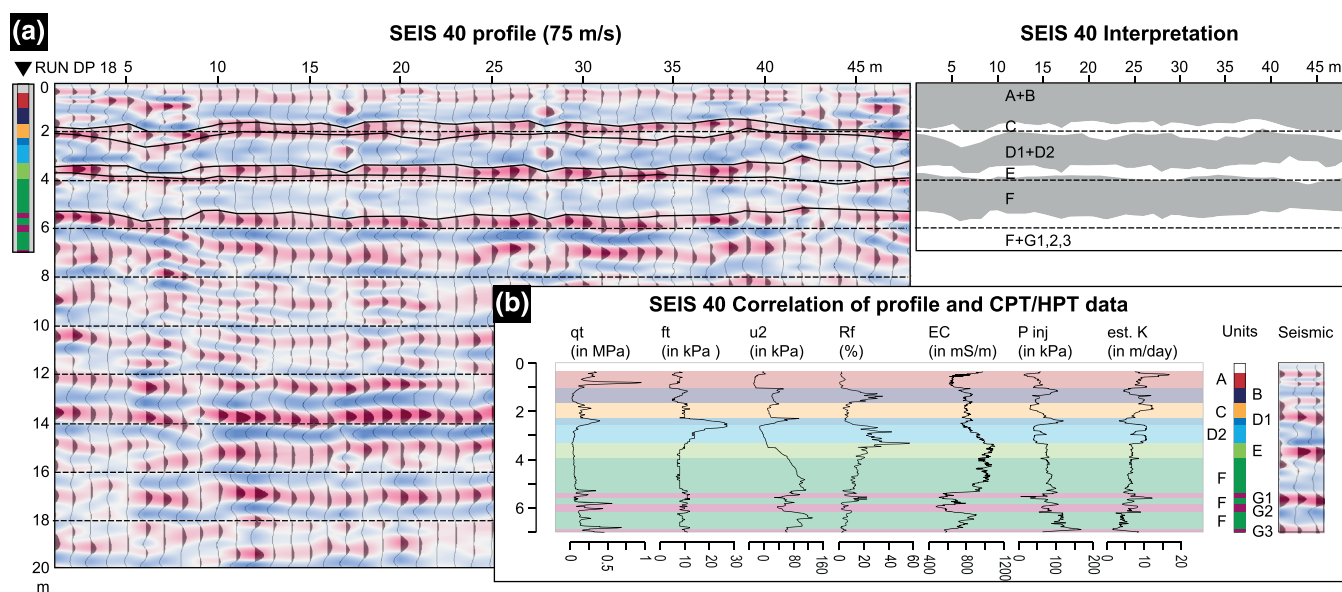
Figure 8(a) shows the resulting zero offset section of profile SEIS 40. Several horizontal layer boundaries are identified in comparison with CPT and HPT data from nearby RUN DP 18 (Figure 8b). Nevertheless, layer thicknesses as identified from CPT/HPT logs are in parts within the range of seismic resolution (Figure 8b, e.g., facies D1 and D2 or G1, F and G2) that can be expected to be more than one fourth of the wavelength, which is the theoretical limit. In Figure 8(b) the discrimination of facies D1 and D2 clearly illustrates the limits of reflection seismic resolution.

Figure 9(a) shows the resulting zero offset section of profile SEIS 41. Again, several horizontally stratified layer boundaries can be identified in comparison to CPT/HPT data of RUN DP 7 (Figure 9b). However, distinct classification of reflection events is more ambiguous than in the example of profile SEIS 40. Main transitions, for example, between the fossil marsh subfacies B and the underlying fossil tidal flat deposits of subfacies C are clearly visible, whereas older/other transitions and layers like the relatively thin fossil marsh subfacies D1 and D2 cannot be distinguished and are visible as a stack of reflections in the seismic data. Below that, the transitions to the pioneer zone and lagoonal subfacies E and F are again clearly visible. Thus, most of the layers show reflection events but are often too thin to be clearly separated.

### 5 | DISCUSSION

#### 5.1 | The Hallig Südfall geo-archive – landscape changes in pre-medieval times

Using a geoscientific standard approach, this study in a first step aimed at deciphering major landscape changes and storm surge impacts in a well-known local historical context. Results show that initially, brackish to marine low-energy conditions (subfacies F) prevail



**FIGURE 8** Seismic profile SEIS 40 ( $75 \text{ m s}^{-1}$ ) (a) and correlation with stratigraphic data from vibracores RUN 17A/18A and Cone Penetration Testing/Hydraulic Profiling Tool (CPT/HPT) logs RUN DP 18 (b) [Color figure can be viewed at [wileyonlinelibrary.com](http://wileyonlinelibrary.com)]

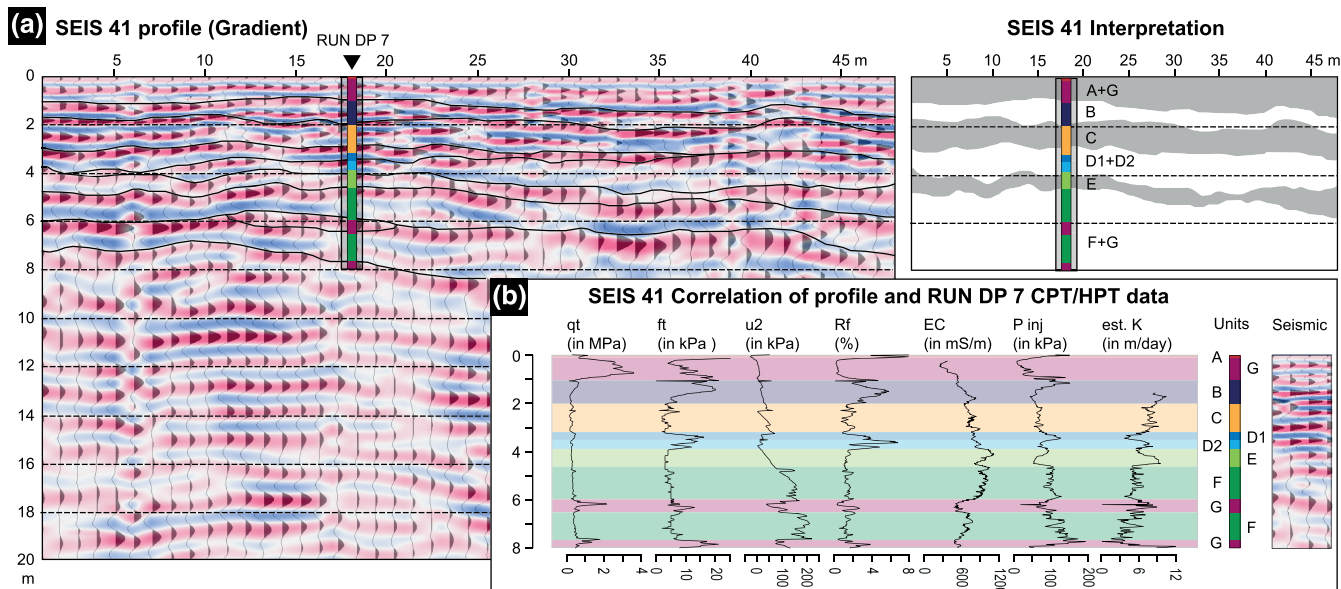


**FIGURE 9** Seismic profile SEIS 41 (gradient) (a) and correlation with stratigraphic data from vibracore RUN 7A and CPT/HPT log RUN DP 7 (b) [Color figure can be viewed at wileyonlinelibrary.com]

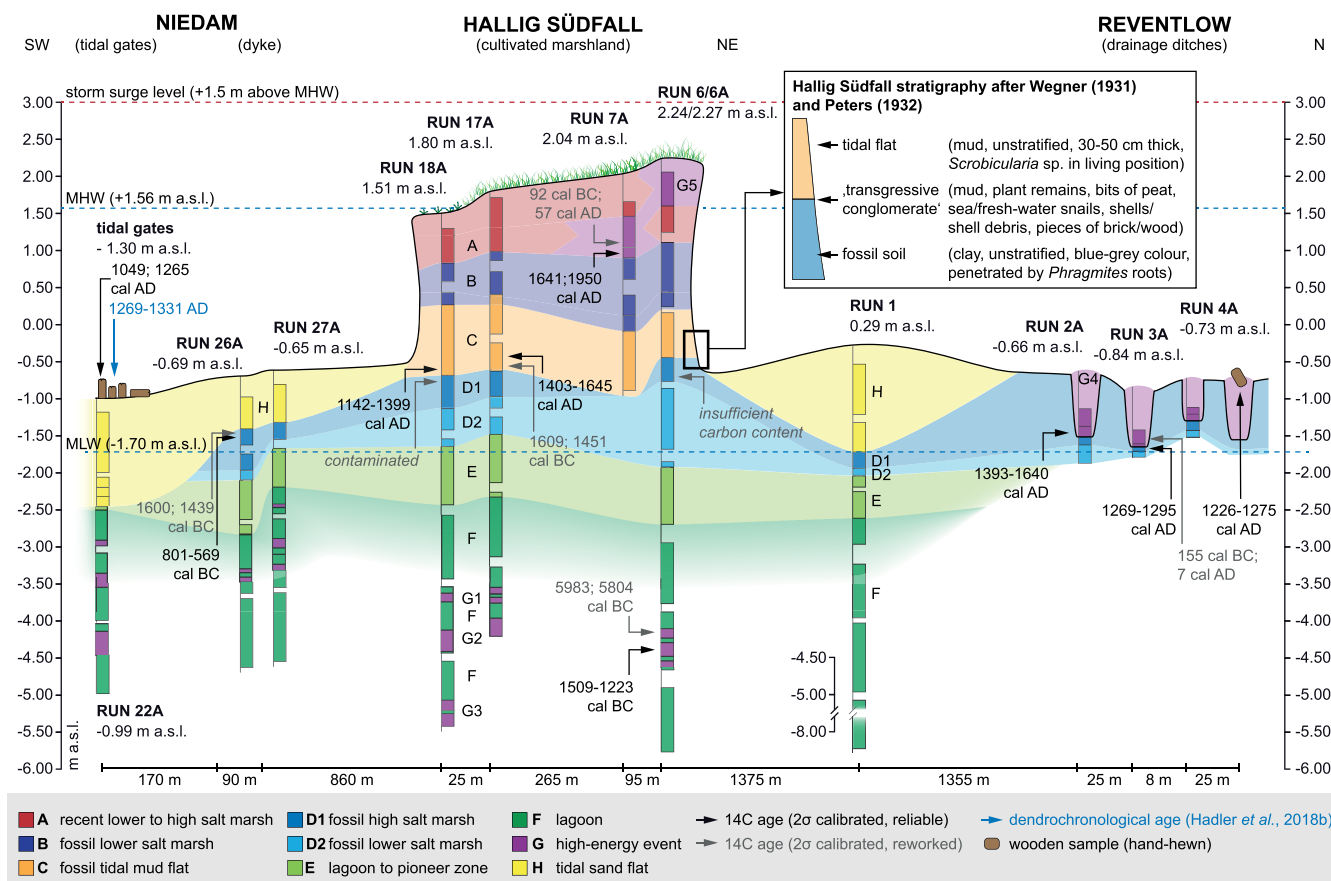


**FIGURE 10** Chronostratigraphic cross section of Hallig Südfall and surrounding tidal flats based on vibracoring, palaeoenvironmental parameter (PEP) analyses, direct push-based sensing data and different dating approaches [Color figure can be viewed at wileyonlinelibrary.com]

throughout the study area (Figure 10). An intersecting shell debris layer (subfacies G) roughly dates this shallow water quiet reach environment to the second millennium BC (1671–1338 cal BC; RUN 6/25 M). Similar layers of sand and/or shell debris (subfacies G) indicate recurring increases in flow dynamics, for example, from tidal inlets or storm surges. Results are thus in good accordance with

Dittmer (1952), Bantelmann (1967) and Hoffmann (2004), who postulate a shallow water lagoonal environment for the second millennium BC.

Facies analysis shows that the water depth continuously decreases due to ongoing sedimentation of silt and clay (subfacies E) while the salinity increases towards fully marine conditions. Subsequently, a



pioneer zone (upper subfacies E) evolves, succeeded by salt marsh formation (subfacies D1, D2). In the surroundings of Südfall, similar fossil soil horizons, developed from homogeneous, grey marine mud incorporating specimens of *Cerastoderma* sp., *Mytilus* sp. and *Peringia* sp. and roots of *Phragmites* sp., were observed by Wegener (1931).

Vertical and thus *in situ* roots penetrate the high salt marsh (subfacies D1) from the former ground surface. Dating to 801 to 569 cal BC (RUN 26A/5 PR), these roots provide a *terminus ante quem* for the marsh formation, that was apparently completed in the early first millennium BC. This fits well to the fact that, for the mid-first millennium BC, Hoffmann (2004) notes the complete absence of any marine influence (i.e., terrestrial conditions) and Dittmer (1952) describes a subsequent widespread formation of fenlands in southern North Frisia.

The fossil marsh complex (subfacies D1, D2, E) is in stratigraphic correlation with relics of fossil marshland found to the north and southwest of Hallig Südfall (Figure 10; Busch, 1923; Hadler & Vött, 2016; Hadler et al., 2018b, 2018c). The extensive reclamation of these marshes only began in the High to Late Middle Ages, though. North of Südfall, finds of pottery, split planks, or metal objects clearly date settlement activities to the 12th to 14th century AD (Kühn, 2016). Towards the southwest, remains of two tidal gates confirm intense cultivation measures for the 11th to 14th century AD (wooden beam A: 1049 to 1265 cal AD, wooden beam C: felling after AD 1331; Niedam area; Figure 10 and Table 2; Hadler et al., 2018a).

So far, results are in good accordance with palaeogeographical scenarios obtained by previous studies in the Wadden Sea region and prove the representability of the Südfall geo-archive for the coastal evolution of North Frisia in pre-medieval times. However, some findings may even provide new insights to the effects of medieval cultivation measures on the coastal landscape.

In the tidal flats around Hallig Südfall, the average medieval surface lies c. -0.85 m a.s.l. (Busch, 1963b). Beneath Hallig Südfall the upper limit of high salt marsh deposits (subfacies D1) reaches up to -0.65 m a.s.l., indicating a better preservation potential. So far, there is no reliable regional sea-level curve for North Frisia (see Bungenstock & Weerts, 2010; Baeteman et al., 2011) but presuming the average present-day sea-level rise of c. 2 mm a<sup>-1</sup> for the North Sea (Hofstede, 1991; BSH, 2020b) and considering some erosion of the topsoil, the cultivated 13th to 14th century AD ground surface lay several decimetres (c. 0.8 m) below the MHW at that time. In nearby places (e.g., Nordstrand peninsula), melioration measures included the extensive extraction of peat overlying the fossil marshes, thus lowering the original medieval ground surface, and causing a stratigraphic gap (Bantelmann, 1967). A similar approach can be assumed for the study area but is so far undocumented. Although dating results are still limited, it may yet be speculated that the age gap of nearly two millennia between marsh formation and land reclamation represents an artificial hiatus and is a result of cultivation. Although further research is needed, this result may indicate a significant human role regarding the increased vulnerability of medieval coastal North Frisia against storm surges.

## 5.2 | The AD 1362 storm surge – historical reports versus geoscientific evidence

So far, there is a significant lack of geoscientific evidence for major coastal changes associated with the major storm surge in AD 1362 and

subsequent coastal evolution. The well-known historic context of the Südfall area provides a promising candidate to compare historical reports and archaeological findings with geoscientific evidence on the post-AD 1362 coastal evolution and to evaluate the reliability of geoscientific results.

The local stratigraphy shows that a tidal mudflat environment (subfacies C) directly succeeds the fossil marshland (subfacies D2) cultivated in medieval times (Figures 3 and 10). A distinct erosive contact marks this transition from terrestrial to (semi-)aquatic conditions, indicating a drastic change of environmental conditions. The frequent occurrence of the infaunal *Scrobicularia plana* in basal subfacies C (RUN 6A, RUN 18A) proves sedimentation below MHW (Willmann, 1989) and hence the permanent flooding of the formerly cultivated marshland. *Scrobicularia plana* was even found burrowed into the upper centimetres of the fossil marsh (subfacies D1, RUN 6A), further emphasizing the drastic change in environmental conditions.

Along the edges of Hallig Südfall, Peters (1932) observed a similar stratigraphy where homogeneous muds with abundant *Scrobicularia* sp. in living position overlie the fossil marsh (Figure 10). Like subfacies C, these muds do not show any layering and are thus interpreted as sediments deposited in a constantly subaquatic environment. Wegener (1931) also described homogeneous clayey fine sands on top of the fossil marsh that he interpreted as tidal mud flat. As our results fit quite well to these early observations, the drastic environmental change from marshland to tidal flats is not a site-specific anomaly at the vibracore location but reflects a development in the whole Südfall area. Peters (1932) further observed a 'transgressive conglomerate' out of mud, peat, marine and terrestrial gastropods, brick fragments and pieces of wood at the contact of fossil marsh (subfacies D1) and tidal flat (subfacies C), that is, a mixture of marine, (semi-)terrestrial and anthropogenic material characteristic for extreme wave events.

We therefore conclude that vibracore stratigraphies from the Südfall geo-archive hold distinct evidence of an extreme event, like a major storm surge, that induced drastic environmental changes by the rapid advance of marine condition into the cultivated marshes of coastal North Frisia. But is this event associated with the AD 1362 storm surge?

An articulated specimen of *Scrobicularia plana* found in subfacies C close to the lower erosive contact of the associated sedimentary unit dates to 1142–1399 cal AD (RUN 18A/10 M), respectively. Considering the stratigraphic position of the sample and the historically reported date of AD 1362, the dating result fits quite well with the storm surge event. An articulated specimen of *Cerastoderma* sp. (RUN 17A M) provides a clear *terminus ante quem* for the storm surge, dating it before 1403–1645 cal AD. Comparable results were also found by Hadler and Vött (2016) and Hadler et al. (2018b) to the north of Hallig Südfall, where former drainage ditches acted as sediment traps for storm surge deposits also associated with the AD 1362 storm event (Reventlow area; Figures 1a and 10 and Table 2).

Given the timeframe, we conclude that the event-related major environmental shift from terrestrial marshland (subfacies D1) to tidal flat conditions (subfacies C) that is preserved beneath Hallig Südfall provides distinct geomorphological evidence of extensive drowning of medieval marshland, most likely by the AD 1362 storm event. The low-lying ground surface thereby favoured the permanent establishment of tidal flats in the study area. This new geoscientific evidence not

only fits very well to the known historical reports on the AD 1362 storm surge but also to archaeological findings from the tidal flats that indicate a sudden end of settlement activities in the 14th century AD (Kühn, 2007).

Subsequently, gradual siltation throughout the newly established tidal flats (subfacies C) induces a second cycle of marsh formation (subfacies B). Results correspond well to historical attempts of a dike building project reaching from the Nordstrand peninsula to Hallig Südfall and to Pellworm (Müller & Fischer, 1936). Such an ambitious project required a silting up of marshland well above MHW and thus attests to post-AD 1362 sedimentation and marsh formation in the wider Südfall area. Locally, this early modern fossil marsh is again overlain by high-energy deposits (subfacies G in RUN 6A/7A) dating to 1641–1950 cal AD (Figures 3 and 10; RUN 7A/10 PR; Hadler et al., 2018b) and/or a third phase of marsh formation (subfacies A). Considering the time frame, it may be speculated, that the deposits belong to one of the major modern era storm surges, for example, the AD 1634 storm surge that finally led to the establishment of the present-day tidal flats around Hallig Südfall. Other candidates could be storm surges in AD 1717 (*Christmas flood*) or AD 1825 (*Große Halligflut* or *February flood*). Subsequently, salt marsh formation (subfacies A) only continued at Hallig Südfall, marking the upper end of the facies sequence and present-day ground surface, while a tidal sand flat (subfacies H) dominates its surroundings.

Summarizing, Hallig Südfall turned out a valuable geo-archive that very well reflects historical reports from medieval to modern times. The local stratigraphy can therefore be considered as representative for the study area and provides a suitable key reference site to test an automated facies identification by statistical analysis of DP-based CPT and HPT sensing data.

### 5.3 | Testing a new approach – facies identification using Direct Push-based Cone Penetration Testing (CPT) and Hydraulic Profiling Tool (HPT) data and linear discriminant analysis (LDA)

Vibracore stratigraphies, PEP analyses and radiocarbon dating allowed a detailed reconstruction of the palaeoenvironmental development of Hallig Südfall from pre-medieval times until today. However, extending such investigations to map the distribution of fossil marshland below the Hallig or in the surrounding tidal flats is very time-consuming and cost intensive. This article therefore aims at the development and test of a new methodological approach for fast and efficient prospection of local stratigraphies by facies interpretation based on data from CPT, the HPT and LDA as well as seismic measurements.

Initial results show that DP-based CPT and HPT data perfectly reflects vibracore stratigraphies and (sub)facies and thus provides a fast and high-resolution tool for palaeoenvironmental investigations. Yet, the accurate interpretation of CPT and HPT logs requires an initial calibration based on vibracores and PEP (Figures 3 and 4).

LDA-based identification of (sub)facies based on DP sensing data worked very well for the RUN DP 18 training data. In fact, 616 out of 666 cases were correctly reclassified, equating to an average reclassification rate of 92.49%. Misclassifications mainly occur close to stratigraphic boundaries between the sedimentary units of two

(sub)facies (Figure 7c). They may, for example, be an effect of CPT logging, as both the sediments ahead and behind the cone have an influence on the measured cone resistance, impeding the exact detection of layer boundaries (Lunne et al., 2002). Most misclassifications (23 cases) affect subfacies F and G and are most likely caused by inaccurate a priori classification of CPT and HPT data due to some interbedding of thin shell debris layers (Figure 3a,b). In 10 cases, subfacies B is mistaken for subfacies C and vice versa. This may be explained by the similarity between tidal mud flat (subfacies C) and lower salt marsh (subfacies B) deposits, as the latter gradually evolves from the former. The proximity of both subfacies types also become evident in Figure 7(a,b). Another 10 misclassifications occur along other facies boundaries and likely result from inaccuracies of a priori grouping. The remaining seven cases are misclassifications in subfacies D1, close to the erosive contact of the associated sedimentary unit. The section equals c. 7 cm in a vertical direction and may be associated with an initial reworking of upper marsh deposits by the high-energy event.

Regarding the RUN DP 7 test dataset, 351 out of 541 cases were correctly classified (average rate of 64.88%) but classification rates vary strongly between (sub)facies. Best results were obtained for subfacies F (98.79%), G (66.67%) and E (41.89%), while the correct group assignment decreases for subfacies D2 (25.64%), D1 (9.68%) and C (6.25%). Most misclassifications occur in subfacies C that is mistaken for subfacies B but also affect the marsh subfacies D1 and – to a minor degree – D2. They are incorrectly assigned to subfacies C. Possible explanations for the observed misclassifications comprise:

- Inaccuracies of a priori grouping. The lateral distance between a vibracoring and DP site increases the likelihood of (sub)facies differences that are passed from the core stratigraphy to the DP-based dataset, leaving some uncertainty concerning the correct depth of facies boundaries.
- Vertical offset in DP-based sensing data. Between HPT and CPT measurements, a minor relocation of the drill rig is necessary. Depending on the local topography and the softness of the surface, the relocation may go hand in hand with a vertical offset of several centimetres between HPT and CPT data. Especially along facies boundaries this offset may cause a shift in values and hence misclassifications but can usually be corrected using distinct peaks for correlation.
- Lateral variations of PEPs within a (sub)facies. Variations in grain size, texture or mineral content likely occur along a transect and may significantly influence DP-based sensing parameters and thereby cause changes in facies classification. As seen in nearby vibracores RUN 6 and 6A, this seems to be the case for the fossil marsh deposits (subfacies D1) that are softer and less consolidated at site RUN DP 7 than corresponding deposits at site RUN DP 18. These changes affect the absolute values of CPT parameters like corrected tip resistance  $q_t$ , corrected sleeve friction  $f_t$  and the dependent friction ratio  $R_f$  and thus may cause a misclassification, here to subfacies C. On the contrary, the well-classified subfacies F and G show little to no lateral variation between coring sites.

Since the grouping inaccuracies and offsets in the DP dataset are well manageable, their influence on classification results can be neglected. Instead, lateral changes of facies type parameters appear

to have a significant influence on LDA-based classifications. Despite low classification rates in the upper part of RUN DP 7, classifications still reflect the overall stratigraphic sequence.

#### 5.4 | Linear discriminant analysis (LDA)-based facies identification as basis for calibrating seismic data

The seismic test datasets presented in this study underline the potential of seismic measurements to extrapolate CPT/HPT logs automatically classified from coring data. Several studies dealt with the application and improvement of electrical resistivity tomography (ERT) to interconnect coring and direct push data (e.g., Wunderlich et al., 2018a). Nevertheless, ERT although constrained by EC logs has its limitations in terms of vertical resolution (which is of the same order as the penetration depth) and contrast, especially in high conductive media. Thus, seismic measurements can be a good supplement for extrapolation of coring data (e.g., Wunderlich et al., 2018b). In unconsolidated, partially saturated soils the velocities of shear-waves are significantly slower than the velocities of compressional waves. Thus, shear-waves typically show a much higher resolution. Furthermore, the shear wave velocity is sensitive to the grain size of a sediment, providing a contrast even for only slight changes in grain size distribution (Schwardt et al., 2020). Our results show that this also accounts for the sedimentary sequence of the study area. Results of profile SEIS 40 clearly reflect the stratigraphy observed from vibracoring and automatically classified CPT/HPT data, whereas the second test site of profile SEIS 41 reflects a more complex image, complicating not only the interpretation of the CPT/HPT data but also seismic data. SEIS 41 shows a larger number of thin layers that are in the order of seismic resolution. To handle this limit of resolution, one could apply full waveform inversion (e.g., Köhn et al., 2019; Schwardt et al., 2020). Nevertheless, this study shows that automatically classified CPT/HPT logs and seismic reflection data complement each other in a way, that – using a suitable training dataset for classification – seismic profiles may be stratigraphically interpreted without associated vibracores and provide another valuable dataset for the detailed palaeoenvironmental reconstruction of a site.

#### 5.5 | Facies classification by Cone Penetration Testing (CPT) and Hydraulic Profiling Tool (HPT) data and linear discriminant analysis (LDA) – a transferable approach

After successfully establishing the LDA-based facies identification of facies from CPT and HPT data for Hallig Südfall, an essential question is the potential and applicability of the new approach for the wider Wadden Sea region, for example, East Frisia in Germany or even the Netherlands or Denmark. As shown, the new approach holds a great potential for the efficient area-wide mapping of different facies in the Hallig Südfall study area. Based on a well-investigated coring site as reference and training dataset, facies can quite reliably be interpreted from CPT and HPT logs using LDA. However, comparing the two locations investigated on Südfall reveals some important aspects that must be considered for the application in other study areas.

As discussed earlier, misclassifications may arise due to the spatial variability of a facies' sedimentological properties. At the same time, other facies may occur in a study area, that were not discovered at the key vibracoring site and so far, not included in the training dataset. To improve the classification as well as reliability of results, it will therefore be essential even for a local study to include more than one vibracore to the training dataset.

We also emphasize that the basic approach of CPT- and HPT-based facies classification using LDA is certainly applicable in the Wadden Sea region or other study areas outside North Frisia (e.g., De Martini et al., 2021), but due to the regional variabilities of facies, a distinct local training dataset must be developed for each study area. Unlike the CPT-based application of soil classification charts (e.g., Robertson, 1990), a certain set of vibracore stratigraphies is needed to apply the enhanced approach of facies identification. Although additional coring again requires a higher amount of time and costs, it is essential to establish a reliable training dataset. The larger the initial dataset, the greater is the potential for a large-scale application and a significant improvement of classification results. Still, DP-based sensing in-between the generally few vibracoring sites of a study area then allows a by far better and more detailed palaeoenvironmental reconstruction than the geoscientific standard approach (Hausmann et al., 2018; Hadler et al., 2020), especially in combination with geophysical prospection.

## 6 | CONCLUSION

Using a geoscientific standard approach of vibracoring, PEP analyses and radiocarbon dating, we were able to reconstruct the palaeogeographical development for the geo-archive Hallig Südfall in the Wadden Sea of North Frisia. Results on the local landscape evolution are in good accordance with historical reports, archaeological findings and preliminary studies. The medieval fossil marsh beneath Südfall was successfully related to known medieval settlement sites in the surrounding tidal flats. Results also point to large scale medieval melioration measures so far only presumed for the Rungholt area. By fossil tidal flat deposits overlying the medieval marshland, the local stratigraphy also provides geoscientific evidence that the AD 1362 storm surge initiated the so far only historically attested major coastal changes leading to the formation of the present day Wadden Sea.

To improve and enhance standard geoscientific research, we introduced a new approach for facies identification using DP-based *in situ* sensing methods (CPT, HPT) combined with LDA. Different facies, defined by PEP analyses, were successfully separated by LDA, thus proving the applicability of CPT and HPT parameters for facies differentiation. Tests on the classification quality, however, emphasize the need to extend the training dataset to more than a single vibracoring site to also consider lateral changes within a facies type. Where CPT and HPT logs indicate significant changes of the local stratigraphy, LDA should be refined by adding additional key vibracoring sites to the training dataset and create a step-by-step improvement of the classification model for the study area. The application of CPT, HPT and LDA can then be used to widely map the distribution of specific facies below Hallig Südfall and in the tidal flats, for example, the distribution of medieval marshland drowned by the AD 1362 storm surge. Based on local training datasets obtained from vibracoring and PEP

analysis, LDA-based facies classification of DP sensing data also provides a promising approach for other study areas in and outside the Wadden Sea region that adds to the geoscientific standard approach. The combination of LDA-based facies classification with geophysical prospection like seismic measurements further allows the spatial extrapolation of automatically classified facies.

## ACKNOWLEDGEMENTS

The German Research Foundation (Deutsche Forschungsgemeinschaft, DFG) is highly acknowledged for funding the RUNGHOLT-project (HA 7647/1-1, VO 938/21-1) and the Central Geophysical Project (RA 496/26-2), that were both part of the DFG-Priority Programme 1630 'Harbours from the Roman Period to the Middle Ages'.

Working permits were kindly issued by the Schleswig-Holstein State Office for Coastal Protection, National Park and Marine Protection (Landesbetrieb für Küstenschutz, Nationalpark und Meeresschutz, Schleswig-Holstein) and the Schleswig-Holstein Archaeological State Office (Archäologisches Landesamt Schleswig-Holstein). The authors are greatly indebted to Gunda and Gonne Erichsen, Hallig Südfall, for transportation and logistic support during fieldwork.

## CONFLICT OF INTEREST

The authors do not have any conflict of interest to declare.

## DATA AVAILABILITY STATEMENT

The data that support the findings of this study are available from the corresponding author upon reasonable request.

## ORCID

Hanna Hadler  <https://orcid.org/0000-0002-5198-1668>

Peter Fischer  <https://orcid.org/0000-0002-8410-5824>

Bente Majchczack  <https://orcid.org/0000-0001-5743-2080>

## REFERENCES

- Athersuch, J., Horne, D.J. & Whittaker, J.E. (1989). *Marine and brackish water ostracods*, Synopses of the British Fauna (New Series), Vol. 43. Leiden, New York, Kobenhaven, Köln: E. J. Brill, pp. 1–359.
- Backhaus, K., Erichson, B., Plinke, W. & Weiber, R. (2016) *Multivariate Analysemethoden. Eine anwendungsorientierte Einführung*. Berlin: Springer-Verlag 10.1007/978-3-662-46076-4.
- Baeteman, C., Waller, M. & Kiden, P. (2011) Reconstructing middle to late Holocene sea-level change: A methodological review with particular reference to 'A new Holocene sea-level curve for the southern North Sea' presented by K.-E. Behre. *Boreas*, 40(4), 557–572. <https://doi.org/10.1111/j.1502-3885.2011.00207.x>
- Bahrenberg, G., Giese, E., Mevenkamp, N. & Nipper, J. (2008) *Statistische Methoden in der Geographie. Band 2: Multivariate Statistik*. Berlin: Borntraeger.
- Bantelmann, A. (1967) Die Landschaftsentwicklung im nordfriesischen Küstengebiet. Eine Funktionschronik durch fünf Jahrtausende. *Die Küste*, 14(2), 5–99.
- Bantelmann, A. (1975) *Die frühgeschichtliche Marschensiedlung beim Elisenhof. Landschaftsgeschichte und Baubefunde*. Bern: Verlag Lang.
- Barsch, H. (Ed). (2000) *Arbeitsmethoden in Physiogeographie und Geoökologie*. Gotha: Klett-Perthes.
- Bartholdy, J. (1997) The backbarrier sediments of the Skallingen Peninsula, Denmark. *Geografisk Tidsskrift - Danish Journal of Geography*, 97(1), 11–32. <https://doi.org/10.1080/00167223.1997.10649389>
- Bartholdy, J. (2012) Salt marsh sedimentation. In: Davis, R.A., Jr. & Dalrymple, R.W. (Eds.) *Principles of tidal sedimentology*. Dordrecht: Springer, pp. 151–185 10.1007/978-94-007-0123-6\_8.
- Bates, M.R., Bates, C.R. & Whittaker, J.E. (2007) Mixed method approaches to the investigation and mapping of buried Quaternary deposits: Examples from southern England. *Archaeological Prospection*, 14(2), 104–129. <https://doi.org/10.1002/arp.303>
- Beefink, W.G. & Rozema, J. (1993) The nature and functioning of salt marshes. In: Salomons, W., Bayne, B.L., Duursma, E.K. & Förstner, U. (Eds.) *Pollution of the North Sea*. Berlin: Springer, pp. 59–87 10.1007/978-3-642-73709-1\_4.
- Begemann, H.K. (1965) The friction jacket cone as an aid in determining the soil profile. In: *Proceedings of the 6th International Conference on Soil Mechanics and Foundation Engineering*, Vol. 1, pp. 17–20.
- Behre, K.E. (2008) A new Holocene sea-level curve for the southern North Sea. *Boreas*, 36(1), 82–102. <https://doi.org/10.1080/03009480600923386>
- Berkeley, A., Perry, C.T., Smithers, S.G., Horton, B.P. & Taylor, K.G. (2007) A review of the ecological and taphonomic controls on foraminiferal assemblage development in intertidal environments. *Earth-Science Reviews*, 83(3–4), 205–230. <https://doi.org/10.1016/j.earscirev.2007.04.003>
- Blott, S.J. & Pye, K. (2001) GRADISTAT: a grain size distribution and statistics package for the analysis of unconsolidated sediments. *Earth Surface Processes and Landforms*, 26(11), 1237–1248. <https://doi.org/10.1002/esp.261>
- Blume, H.-P., Stahr, K. & Leinweber, P. (2011) *Bodenkundliches Praktikum*. Heidelberg: Spektrum Akademischer Verlag.
- Boden, A.-h.-A. (2005) *Bodenkundliche Kartieranleitung*. Stuttgart: Schweizerbart.
- Brückner, H. & Gerlach, R. (2020) Geoarchäologie. In: Gebhardt, H., Glaser, R., Radtke, U., Reuber, P. & Vött, A. (Eds.) *Geographie. Physische Geographie und Humangeographie*, Vol. 3. Auflage. Berlin: Springer Nature, pp. 447–453.
- BSH - Bundesamt für Seeschifffahrt und Hydrographie. (2020a) Pegelinformation Südfall, Fahrwasserkante. Available at: [https://tableau.bsh.de/views/Gezeitenvorausberechnung/Gezeitenvorausbe-rechnung\\_Einzelpegel?Kurzname=S%C3%BCdfall&Bezugsniveau=Seekartennull%20\(SKN\)&Zeiten=Gesetzliche%20Zeit%20\(Sommer:%20MESZ%20%20Winter:%20MEZ\)&pixelratio=2&embed=y&:showAppBanner=false&:display\\_count=no&:showVizHome=no&:alerts=no&:tabs=no&:showShareOptions=true&:toolbar=yes](https://tableau.bsh.de/views/Gezeitenvorausberechnung/Gezeitenvorausbe-rechnung_Einzelpegel?Kurzname=S%C3%BCdfall&Bezugsniveau=Seekartennull%20(SKN)&Zeiten=Gesetzliche%20Zeit%20(Sommer:%20MESZ%20%20Winter:%20MEZ)&pixelratio=2&embed=y&:showAppBanner=false&:display_count=no&:showVizHome=no&:alerts=no&:tabs=no&:showShareOptions=true&:toolbar=yes) [accessed 29 October 2020].
- BSH - Bundesamt für Seeschifffahrt und Hydrographie. (2020b) Relativer Meeresspiegel. Zeitreihe des monatlichen Wasserstandes am Pegel Cuxhaven Steubenhöft. Available at: [https://www.bsh.de/DE/DATEN/Wasserstand\\_Nordsee/Meeresspiegelschwankungen/meeresspiegelschwankungen\\_node.html](https://www.bsh.de/DE/DATEN/Wasserstand_Nordsee/Meeresspiegelschwankungen/meeresspiegelschwankungen_node.html) [accessed 29 October 2020].
- Bungenstock, F. & Schäfer, A. (2009) The Holocene relative sea-level curve for the tidal basin of the barrier island Langeoog, German Bight, southern North Sea. *Global and Planetary Change*, 66(1-2), 34–51. <https://doi.org/10.1016/j.jglplacha.2008.07.007>
- Bungenstock, F. & Weerts, H.J. (2010) The high-resolution Holocene sea-level curve for northwest Germany: global signals, local effects or data-artefacts? *International Journal of Earth Sciences*, 99(8), 1687–1706. <https://doi.org/10.1007/s00531-009-0493-6>
- Busch, A. (1923) Die Entdeckung der letzten Spuren Rungholts. *Jahrbuch Des Nordfriesischen Vereins für Heimatkunde*, 10, 1–32.
- Busch, A. (1962) *Die heutige Hallig Südfall und die letzten Spuren Rungholts und über Clades Rungholtina*. Neumünster: Karl Wachholtz Verlag.
- Busch, A. (1963a) Zur Rekonstruktion der Rungholter Schleusen. *Die Heimat*, 70(6), 163–170.
- Busch, A. (1963b) Alte und neue Deichprofile von Strucklahnungshörn (Nordstrand) und der Anstieg des Meeresspiegels. *Die Heimat*, 70, 4–10.
- Chagué-Goff, C., Goff, J., Wong, H.K. & Cisternas, M. (2015) Insights from geochemistry and diatoms to characterise a tsunami's deposit and maximum inundation limit. *Marine Geology*, 359, 22–34. <https://doi.org/10.1016/j.margeo.2014.11.009>
- Chagué-Goff, C., Szczuciński, W. & Shinozaki, T. (2017) Applications of geochemistry in tsunami research: A review. *Earth-Science Reviews*, 165, 203–244. <https://doi.org/10.1016/j.earscirev.2016.12.003>

- Croudace, I.W., Rindby, A. & Rothwell, R.G. (2006) ITRAX: description and evaluation of a new multi-function X-ray core scanner. *Geological Society of London, Special Publication*, 267(1), 51–63. <https://doi.org/10.1144/GSL.SP.2006.267.01.04>
- De Martini, P.M., Bruins, H.J., Feist, L., Goodman-Tchernov, B.N., Hadler, H. & Lario, J. (2021) The Mediterranean Sea and the Gulf of Cadiz as a natural laboratory for paleotsunami research: Recent advancements. *Earth-Science Reviews*, 216, 103578. <https://doi.org/10.1016/j.earscirev.2021.103578>
- Dearing, J. (1999) Environmental Magnetic Susceptibility. In: *Using the Bartington MS2 System*. Kenilworth: Chi Publications.
- Dearing, J.A., Hay, K.L., Baban, S.M.J., Huddleston, A.S., Wellington, E.M. H. & Loveland, P. (1996) Magnetic susceptibility of soil: an evaluation of conflicting theories using a national data set. *Geophysical Journal International*, 127(3), 728–734. <https://doi.org/10.1111/j.1365-246X.1996.tb04051.x>
- Dittmer, E. (1952) Die nacheiszeitliche Entwicklung der schleswig-holsteinischen Westküste. *Meyniana*, 1, 138–168.
- Douglas, B.J. & Olsen, R.S. (1981) Soil Classification Using Electric Cone Penetrometer. In: *Proceedings of Conference on Cone Penetration Testing and Experience*, St Louis, MO, USA, 26–30 October 1981, 209–227.
- Edwards, R.J. & Horton, B.P. (2000) Reconstructing relative sea-level change using UK salt-marsh foraminifera. *Marine Geology*, 169(1–2), 41–56. [https://doi.org/10.1016/S0025-3227\(00\)00078-5](https://doi.org/10.1016/S0025-3227(00)00078-5)
- Enters, D., Haynert, K., Wehrmann, A., Freund, H. & Schlütz, F. (2021) A new  $\Delta R$  value for the southern North Sea and its application in coastal research. *Netherlands Journal of Geosciences*, 100, e1. <https://doi.org/10.1017/njg.2020.19>
- EPA - United States Environmental Protection Agency. (2007) Field Portable X-Ray Fluorescence Spectrometry for the Determination of Elemental Concentrations in Soil and Sediment. Available at: <https://www.epa.gov/sites/production/files/2015-12/documents/6200.pdf> [accessed 29 October 2020].
- Evans, M. & Heller, F. (2003) *Environmental magnetism: Principles and applications of enviromagnetics*. Sandiego: Academic Press.
- Finkler, C., Fischer, P., Baika, K., Rigakou, D., Metallinou, G., Hadler, H. & Vött, A. (2018) Tracing the Alkinoos Harbor of ancient Kerkyra, Greece, and reconstructing its paleotsunami history. *Geoarchaeology*, 33(1), 24–42. <https://doi.org/10.1002/gea.21609>
- Fischer, O. & Müller, F. (1936) *Das Wasserwesen an der schleswig-holsteinischen Nordseeküste. Die Inseln*, Vol. 2. Berlin: Verlag Dietrich Reimer.
- Fischer, P., Hilgers, A., Protze, J., Kels, H., Lehmkuhl, F. & Gerlach, R. (2012) Formation and geochronology of Last Interglacial to Lower Weichselian loess/palaeosol sequences – case studies from the Lower Rhine Embayment, Germany. *Eiszeitalter Und Gegenwart*, 61, 48–63. <https://doi.org/10.3285/eg.61.1.04>
- Fischer, P., Wunderlich, T., Rabbel, W., Vött, A., Willershäuser, T., Baika, K., et al. (2016) Combined electrical resistivity tomography (ERT), direct-push electrical conductivity (DP-EC) logging and coring. A new methodological approach in geoarchaeological research. *Archaeological Prospection*, 23(3), 213–228. <https://doi.org/10.1002/arp.1542>
- Fischer, P., Zielhofer, C. & Vött, A. (2020) Exkurs 5.2: Direct-Push-Verfahren in der Geomorphologie. In: Gebhardt, H., Glaser, R., Radtke, U., Reuber, P. & Vött, A. (Eds.) *Geographie. Physische Geographie und Humangeographie*. Berlin: Springer Nature, pp. 96–97.
- Frenzel, P., Ewald, J. & Pint, A. (2017) Salinity-dependent sieve pore variability in *Cyprideis torosa*: An experiment. *Journal of Micro-palaeontology*, 36(1), 57–62. <https://doi.org/10.1144/jmpaleo2016-009>
- Frenzel, P., Keyser, D. & Viehberg, F.A. (2010) An illustrated key and (palaeo) ecological primer for postglacial to recent Ostracoda (Crustacea) of the Baltic Sea. *Boreas*, 39(3), 567–575. <https://doi.org/10.1111/j.1502-3885.2009.00135.x>
- Frenzel, P., Schulze, I. & Pint, A. (2012) Noding of *Cyprideis torosa* valves (Ostracoda) – a proxy for salinity? New data from field observations and a long-term microcosm experiment. *International Review of Hydrobiology*, 97(4), 314–329. <https://doi.org/10.1002/iroh.201211494>
- Fruergaard, M., Møller, I., Johannessen, P.N., Nielsen, L.H., Andersen, T.J., Nielsen, L., et al. (2015) Stratigraphy, evolution, and controls of a Holocene transgressive–regressive barrier island under changing sea level: Danish North Sea coast. *Journal of Sedimentary Research*, 85(7), 820–844. <https://doi.org/10.2110/jsr.2015.53>
- Gehrels, W.R. & Newman, S.W. (2004) Salt-marsh foraminifera in Ho Bugt, western Denmark, and their use as sea-level indicators. *Geografisk Tidsskrift-Danish Journal of Geography*, 104(1), 97–106. <https://doi.org/10.1080/00167223.2004.10649507>
- Geoprobe. (2015) Geoprobe Hydraulic Profiling Tool (HPT) System. Standard Operating Procedure. Available at: [https://geoprobe.com/sites/default/files/storage/pdfs/HPT\\_SOP\\_mk3010\\_0115\\_0.pdf](https://geoprobe.com/sites/default/files/storage/pdfs/HPT_SOP_mk3010_0115_0.pdf) [accessed 29 October 2020].
- Goldberg, P. & Macphail, R. (2006) *Practical and theoretical geoarchaeology*. Oxford: Blackwell Publishing.
- Hadler, H., Fediuk, A., Fischer, P., Rabbel, W., Schwardt, M., Wilken, D., et al. (2018a) Drowned by the Grote Mandränke in 1362 AD – new geo-archaeological research on the late medieval trading centre Rungholt (North Frisia). In: Egberts, L. & Schroor, M. (Eds.) *Waddenland Outstanding – History, Landscape and Cultural Heritage of the Wadden Sea Region*. Amsterdam: University Press Amsterdam, pp. 239–252.
- Hadler, H., Fischer, P., Obrocki, L., Heinzelmann, M. & Vött, A. (2020) River channel evolution and tsunami impacts recorded in local sedimentary archives – the ‘Fiume Morto’ at Ostia Antica (Tiber River, Italy). *Sedimentology*, 67(3), 1309–1343. <https://doi.org/10.1111/sed.12599>
- Hadler, H. & Vött, A. (2016) Das Rungholt-Watt im Fokus aktueller geoarchäologischer Forschungen. In: Newig, J. & Haupenthal, U. (Eds.) *Rungholt – rätselhaft und widersprüchlich*. Husum: Husum Druck- und Verlagsgesellschaft, pp. 118–120.
- Hadler, H., Vött, A., Newig, J., Emde, K., Finkler, C., Fischer, P. & Willershäuser, T. (2018b) Geoarchaeological evidence of marshland destruction in the area of Rungholt, present-day Wadden Sea around Hallig Südfall (North Frisia, Germany), by the Grote Mandränke in 1362 AD. *Quaternary International*, 473, 37–54. <https://doi.org/10.1016/j.quaint.2017.09.013>
- Hadler, H., Wilken, D., Willershäuser, T., Schwardt, M., Fediuk, A., Werner, V., et al. (2018c) Auf den Spuren Rungholts – Geoarchäologische Untersuchungen im Wattgebiet um Hallig Südfall (Nordfriesland). *Archäologische Nachrichten Aus Schleswig-Holstein*, 24, 86–99.
- Hanesch, M. & Scholger, R. (2005) The influence of soil type on the magnetic susceptibility measured throughout soil profiles. *Geophysical Journal International*, 161(1), 50–56. <https://doi.org/10.1111/j.1365-246X.2005.02577.x>
- Hausmann, J., Zielhofer, C., Werther, L., Berg-Hobohm, S., Dietrich, P., Heymann, R. & Werban, U. (2018) Direct push sensing in wetland (geo) archaeology: High-resolution reconstruction of buried canal structures (Fossa Carolina, Germany). *Quaternary International*, 473, 21–36. <https://doi.org/10.1016/j.quaint.2017.02.008>
- Heaton, T.J., Köhler, P., Butzin, M., Bard, E., Reimer, R.W., Austin, W.E., et al. (2020) Marine20 - the marine radiocarbon age calibration curve (0–55,000 cal BP). *Radiocarbon*, 62(4), 779–820. <https://doi.org/10.1017/RDC.2020.68>
- Hecht, F. (1933) Der Verbleib der organischen Substanz der Tiere bei meeresischer Einbettung. *Senckenbergiana*, 15(3/4), 167–249.
- Heimreich, A. (1982) *Nordfriesische Chronick. Unveränderter Nachdruck der Ausgabe Tondern 1819, ergänzt um den Innentitel der 2. Ausgabe, Schleswig 1668*. Leer: Verlag Schuster.
- Heywood, B.R., Bazylinski, D.A., Garratt-Reed, A., Mann, S. & Frankel, R.B. (1990) Controlled biosynthesis of greigite (Fe<sub>3</sub>S<sub>4</sub>) in magnetotactic bacteria. *Naturwissenschaften*, 77(11), 536–538. <https://doi.org/10.1007/BF01139266>
- Higelke, B., Hoffmann, D. & Müller-Wille, M. (1982) Das Norderhever-Projekt. Beiträge zur Landschafts- und Siedlungsgeschichte der nordfriesischen Marschen und Watten im Einzugsbereich. *Offa*, 39, 245–270.

- Hilton, J. (1990) Greigite and the magnetic properties of sediments. *Limnology and Oceanography*, 35(2), 509–520. <https://doi.org/10.4319/lo.1990.35.2.0509>
- Hoffmann, D. (2004) Holocene landscape development in the marshes of the west coast of Schleswig-Holstein, Germany. *Quaternary International*, 112(1), 29–36. [https://doi.org/10.1016/S1040-6182\(03\)00063-6](https://doi.org/10.1016/S1040-6182(03)00063-6)
- Hoffmann, D., Kühn, H.J. & Higelke, B. (1984) Landschafts- und Siedlungsgeschichte im Bereich der heutigen Marscheninseln und Watten Nordfriesland. *Siedlungsforschung*, 2, 165–185.
- Hofstede, J.L.A. (1991) Sea-level rise in the inner German Bight (Germany) since AD 600 and its implications upon tidal flats geomorphology. In: Brückner, H. & Radtke, U. (Eds.) *Von der Nordsee bis zum Indischen Ozean*. Stuttgart: Steiner Verlag, pp. 11–27.
- Horton, B.P. & Edwards, R.J. (2006) Quantifying Holocene sea level change using intertidal foraminifera: lessons from the British Isles. *Cushman Foundation Special Publication*, 40, 1–97. [https://doi.org/10.11137/2006\\_1\\_541-542](https://doi.org/10.11137/2006_1_541-542)
- Horton, B.P., Edwards, R.J. & Lloyd, J.M. (1999) UK intertidal foraminiferal distributions: Implications for sea-level studies. *Marine Micropaleontology*, 36(4), 205–223. [https://doi.org/10.1016/S0377-8398\(99\)00003-1](https://doi.org/10.1016/S0377-8398(99)00003-1)
- Hutton, J.T. (1977) Titanium and zirconium minerals. In: Dixon, L.B. (Ed.) *Minerals in Soil Environments*. Soil Science Society of America: Madison, WI, pp. 673–688.
- Ickerodt, U., Kloöß, S., Maluck, M., Siegloff, E., Tummuscheit, A. & Fischer, J. (2017) Archäologische Denkmalpflege im Nordfriesischen Wattenmeer. *Die Heimat*, 124(11/12), 205–214.
- Jefferies, M.G. & Davies, M.P. (1993) Use of CPTU to estimate equivalent SPT N 60. *Geotechnical Testing Journal*, 16(4), 458–468. <https://doi.org/10.1520/GTJ10286J>
- Judd, K., Chagué-Goff, C., Goff, J., Gadd, P., Zawadzki, A. & Fierro, D. (2017) Multi-proxy evidence for small historical tsunamis leaving little or no sedimentary record. *Marine Geology*, 385, 204–215. <https://doi.org/10.1016/j.margeo.2017.01.002>
- Kabata-Pendias, A. (2011) *Trace Elements in Soils and Plants*. Boca Raton, FL: CRC Press.
- Köhn, D., Wilken, D., De Nil, D., Wunderlich, T., Rabbel, W., Werther, L., et al. (2019) Comparison of time-domain SH waveform inversion strategies based on sequential low and bandpass filtered data for improved resolution in near-surface prospecting. *Journal of Applied Geophysics*, 160, 69–83. <https://doi.org/10.1016/j.jappgeo.2018.11.001>
- Köhn, M. (1929) Korngrößenanalyse mittels Pipettanalyse. *Tonindustrie-Zeitung*, 53, 729–731.
- Koster, K. (2016) Cone Penetration Testing: A sound method for urban archaeological prospection. *Archaeological Prospection*, 23(1), 55–69. <https://doi.org/10.1002/arp.1531>
- Kremer, B.P. (2001) Im Einfluss der Gezeiten. Salzwiesen: Leben zwischen Land und Meer. *Biologie in Unserer Zeit*, 31(4), 240–248. [https://doi.org/10.1002/1521-415X\(200104\)31:4<240::AID-BIUZ240>3.0.CO;2-Z](https://doi.org/10.1002/1521-415X(200104)31:4<240::AID-BIUZ240>3.0.CO;2-Z)
- Kühn, H.J. (2007) Jenseits der Deiche. Archäologie im nordfriesischen Wattenmeer. In: Carnap-Bornheim, C. & Radtke, C. (Eds.) *Es war einmal ein Schiff*. Hamburg: Marebuchverlag, pp. 251–284.
- Kühn, H.J. (2016) Die archäologischen Funde aus dem Rungholt-Watt. In: Newig, J. & Hauptenthal, U. (Eds.) *Rungholt. Rätselhaft und widersprüchlich*. Husum: Husum Druck- und Verlagsgesellschaft, pp. 125–167.
- Kühn, H.J. & Panten, A. (1989) *Der frühe Deichbau in Nordfriesland. Archäologisch-historische Untersuchungen*. Bredstedt: Verlag Nordfriisk Instituut.
- Lehmann, G. (2000) Vorkommen, Populationsentwicklung, Ursache fleckenhafter Besiedlung und Fortpflanzungsbiologie von Foraminiferen in Salzwiesen und Flachwasser der Nord- und Ostseeküste Schleswig-Holsteins. Thesis, Kiel, Christian-Albrechts Universität. Available at: [https://macau.uni-kiel.de/receive/diss\\_mods\\_00000413?lang=de](https://macau.uni-kiel.de/receive/diss_mods_00000413?lang=de) [accessed 29 October 2020].
- Lindhorst, S., Betzler, C. & Hass, H.C. (2008) The sedimentary architecture of a Holocene barrier spit (Sylt, German Bight): Swash-bar accretion and storm erosion. *Sedimentary Geology*, 206(1–4), 1–16. <https://doi.org/10.1016/j.sedgeo.2008.02.008>
- LKN Landesbetrieb für Küstenschutz, Nationalpark und Meeresschutz Schleswig-Holstein, Fachbereich Hydrologie, Mess- und Beobachtungsdienst. (2019) Data for perennial tide gauge Everschop, 1977–2018. Unpublished data.
- LLUR Landesamt für Landwirtschaft, Umwelt und ländliche Räume des Landes Schleswig Holstein. (2012) Die Böden Schleswig-Holsteins. Schriftenreihe LLUR SH – GB 23. Available at: [https://www.umweltdaten.landsh.de/nuis/upool/gesamt/geologie/bodenbroschuere\\_2019.pdf](https://www.umweltdaten.landsh.de/nuis/upool/gesamt/geologie/bodenbroschuere_2019.pdf) [accessed 29 October 2020].
- Lunne, T., Robertson, P.K. & Powell, J.J.M. (2002) *Cone Penetration Testing in Geotechnical Practice*. London/New York: Taylor and Francis Group 10.1201/9781482295047.
- Mann, S., Sparks, N.H., Frankel, R.B., Bazylinski, D.A. & Jannasch, H.W. (1990) Biomineralization of ferrimagnetic greigite (Fe<sub>3</sub>S<sub>4</sub>) and iron pyrite (FeS<sub>2</sub>) in a magnetotactic bacterium. *Nature*, 343(6255), 258–261. <https://doi.org/10.1038/343258a0>
- Meijles, E.W., Kiden, P., Streurman, H.-J., van der Plicht, J., Vos, P.C., Gehrels, W.R. & Kopp, R.E. (2018) Holocene relative mean sea-level changes in the Wadden Sea area, northern Netherlands. *Journal of Quaternary Science*, 33, 905–923. <https://doi.org/10.1002/jqs.3068>
- Meyers, S.R. <http://www.geology.wisc.edu/~smeyers/software.html>
- Möller, T. (1926) Eine Fahrt nach Rungholt. *Nordelbingen*, 5, 402–421.
- Müller, F. & Fischer, O. (1936) Alt-Nordstrand bis zur Zerstörung durch die Sturmflut im Jahre 1634. In: *Das Wasserwesen an der schleswig-holsteinischen Nordseeküste. Zweiter Teil: Die Inseln*. Berlin: Verlag von Dietrich Reimer.
- Müller, W. (1958) Grundsätzliche Betrachtungen zur systematischen Gliederung der Marschböden. *Geologisches Jahrbuch*, 76, 11–24.
- Müller-Navarra, K. (2018) Salt-marsh foraminifera and their potential for sea-level studies in the North Sea region. Thesis, Hamburg, Universität Hamburg, viewed January 2018, ediss.sub.hamburg.
- Müller-Navarra, K., Milker, Y., Bunzel, D., Lindhorst, S., Friedrich, J., Arz, H. & Schmiedl, G. (2019) Evolution of a salt marsh in the south-eastern North Sea region—anthropogenic and natural forcing. *Estuarine, Coastal and Shelf Science*, 218, 268–277. <https://doi.org/10.1016/j.ecss.2018.12.022>
- Müller-Navarra, K., Milker, Y. & Schmiedl, G. (2016) Natural and anthropogenic influence on the distribution of salt marsh foraminifera in the bay of Tümlau, German North Sea. *The Journal of Foraminiferal Research*, 46(1), 61–74. <https://doi.org/10.2113/gsjfr.46.1.61>
- Müller-Navarra, K., Milker, Y. & Schmiedl, G. (2017) Applicability of transfer functions for relative sea-level reconstructions in the southern North Sea coastal region based on salt-marsh foraminifera. *Marine Micropaleontology*, 135, 15–31. <https://doi.org/10.1016/j.marmicro.2017.06.003>
- Murray, J.W. (1971) *An Atlas of British Recent Foraminiferids*. London: Heinemann Educational Books.
- Murray, J.W. (2006) *Ecology and Application of Benthic Foraminifera*. Cambridge: Cambridge University Press 10.1017/CBO9780511535529.
- Newig, J. (2004) Die Küstengestalt Nordfrieslands im Mittelalter nach historischen Quellen. *Coastline Reports*, 1, 23–36.
- Newig, J. (2014) Nordfrieslands Küste zwischen Landgewinn und Landverlust. *Geographische Rundschau*, 66(3), 4–13.
- Newig, J. & Hauptenthal, U. (Eds.) (2016) *Rungholt. Rätselhaft und widersprüchlich*. Husum: Husum Druck- u. Verlagsgesellschaft.
- Obrocki, L., Vött, A., Wilken, D., Fischer, P., Willershäuser, T., Koster, B., et al. (2020) Tracing tsunami signatures of the ad 551 and ad 1303 tsunamis at the Gulf of Kyparissia (Peloponnese, Greece) using direct push in situ sensing techniques combined with geophysical studies. *Sedimentology*, 67(3), 1274–1308. <https://doi.org/10.1111/sed.12555>
- Penney, D.N. (1987) Application of Ostracoda to sea-level studies. *Boreas*, 16(3), 237–247. <https://doi.org/10.1111/j.1502-3885.1987.tb00092.x>
- Peters, L.C. (1932) Neues vom schwindenden Rungholt. *Die Heimat*, 42(12), 284–287.
- Petersen, M. & Rohde, H. (1977) *Sturmflut: die grossen Fluten an den Küsten Schleswig-Holsteins und in der Elbe*. Kiel: Wachholtz.
- Pint, A., Frenzel, P., Fuhrmann, R., Scharf, B. & Wennrich, V. (2012) Distribution of *Cyprideis torosa* (Ostracoda) in Quaternary athalassic

- sediments in Germany and its application for palaeoecological reconstructions. *International Review of Hydrobiology*, 97(4), 330–355. <https://doi.org/10.1002/iroh.201111495>
- Polderman, P.J.G. (1974) The Oribatida (Acari) of saline areas in the western part of the Dutch Wadden Sea. *Netherlands Journal of Sea Research*, 8(1), 49–72. [https://doi.org/10.1016/0077-7579\(74\)90026-X](https://doi.org/10.1016/0077-7579(74)90026-X)
- R Core Team. (2014) *R: A Language and Environment for Statistical Computing*. Vienna: R Foundation for Statistical Computing.
- Rabiger-Völlmer, J., Schmidt, J., Linzen, S., Schneider, M., Werban, U., Dietrich, P., et al. (2020) Non-invasive prospection techniques and direct push sensing as high-resolution validation tools in wetland geoarchaeology—Artificial water supply at a Carolingian canal in south Germany? *Journal of Applied Geophysics*, 173, 103928. <https://doi.org/10.1016/j.jappgeo.2019.103928>
- Rauterberg, C. (2000) Alte Kirchen in Nordfriesland. In: Steensen, H. (Ed.) *Das große Nordfriesland-Buch*. Hamburg: Ellen & Richter.
- Reimer, P.J., Austin, W.E., Bard, E., Bayliss, A., Blackwell, P.G., Ramsey, C.B., et al. (2020) The IntCal20 northern hemisphere radiocarbon age calibration curve (0–55 cal kBP). *Radiocarbon*, 62(4), 725–757. <https://doi.org/10.1017/RDC.2020.41>
- Reineck, H.E. (1982) *Das Watt. Ablagerungs- und Lebensraum*. Frankfurt/Main: W. Kramer Verlag.
- Reineck, H.E. & Singh, I.B. (1980) *Depositional Sedimentary Environments*. Berlin, Heidelberg: Springer.
- Richter, T.O., Van der Gaast, S., Koster, B., Vaars, A., Gieles, R., de Stigter, H.C., et al. (2006) The Avaatech XRF Core Scanner: technical description and applications to NE Atlantic sediments. *Geological Society of London, Special Publication*, 267(1), 39–50. <https://doi.org/10.1144/GSL.SP.2006.267.01.03>
- Robertson, P.K. (1990) Soil classification using the cone penetration test. *Canadian Geotechnical Journal*, 27(1), 151–158. <https://doi.org/10.1139/t90-014>
- Robertson, P.K. (2009) Interpretation of cone penetration tests – a unified approach. *Canadian Geotechnical Journal*, 46(11), 1337–1355. <https://doi.org/10.1139/T09-065>
- Rosenfeld, A. & Vesper, B. (1976) The variability of the sieve-pores in Recent and fossil species of *Cyprideis torosa* (Jones, 1850) as an indicator for salinity and palaeosalinity. In: Löffler, H. & Danielopol, D. (Eds.) *Aspects of Ecology and Zoogeography of Recent and Fossil Ostracoda*. The Hague: Junk, pp. 55–67.
- Rothwell, R.G. (2015) Twenty years of XRF core scanning marine sediments: What do geochemical proxies tell us? In: Croudace, I.W. & Rothwell, R.G. (Eds.) *Micro-XRF Studies of Sediment Cores: Applications of a non-destructive tool for the environmental sciences*. Dordrecht: Springer, pp. 25–102. [10.1007/978-94-017-9849-5\\_2](https://doi.org/10.1007/978-94-017-9849-5_2)
- Rothwell, R.G., Hoogakker, B., Thomson, J., Croudace, I.W. & Frenz, M. (2006) Turbidite emplacement on the southern Balearic Abyssal Plain (western Mediterranean Sea) during Marine Isotope Stages 1–3: an application of ITRAX XRF scanning of sediment cores to lithostratigraphic analysis. *Geological Society London Special Publications*, 267(1), 39–50.
- Russell, N., Cook, G.T., Ascough, P.L. & Dugmore, A.J. (2010) Spatial variation in the marine radiocarbon reservoir effect throughout the Scottish post-Roman to Late Medieval period: North Sea values (500–1350 BP). *Radiocarbon*, 52(3), 1166–1181. <https://doi.org/10.1017/S0033822200046245>
- Schäfer, A. (2020) *Klastische Sedimente: Fazies und Sequenzstratigraphie*. Berlin: Springer-Spektrum.
- Scheder, J., Frenzel, P., Bungenstock, F., Engel, M., Brueckner, H. & Pint, A. (2019) Vertical and lateral distribution of Foraminifera and Ostracoda in the East Frisian Wadden Sea—developing a transfer function for relative sea-level change. *Geologica Belgica*, 22(3/4), 99–110. <https://doi.org/10.20341/gb.2019.007>
- Scheffer, F. & Schachtschabel, P. (2018) *Lehrbuch der Bodenkunde*. Heidelberg: Spektrum Akademischer Verlag.
- Schindler, M., Karius, V., Arns, A., Deicke, M. & von Eynatten, H. (2014a) Measuring sediment deposition and accretion on anthropogenic marshland—Part II: The adaptation capacity of the North Frisian Halligen to sea level rise. *Estuarine, Coastal and Shelf Science*, 151, 246–255. <https://doi.org/10.1016/j.ecss.2014.08.027>
- Schindler, M., Karius, V., Deicke, M. & von Eynatten, H. (2014b) Measuring sediment deposition and accretion on anthropogenic marshland—Part I: Methodical evaluation and development. *Estuarine, Coastal and Shelf Science*, 151, 236–245. <https://doi.org/10.1016/j.ecss.2014.08.029>
- Schmidt, W. & Scheibner, H. (1988) Zur Bestimmung des Gehaltes an organischer Substanz von Torfen und Mudden. *Archiv Acker-Und Pflanzenbau Und Bodenkunde*, 32, 423–433.
- Schoch, W.H., Pawlik, B. & Schweingruber, F.H. (1988) *Botanische Makroreste*. Bern: Paul Haupt.
- Schroeder, D. & Brümmer, G. (1968) Zur Genese und Klassifizierung der Marschen. *Mitteilungen der Deutschen Bodenkundlichen Gesellschaft*, 8, 243–245.
- Schrott, L. (2015) Gelände-Arbeitsmethoden in der Geomorphologie. In: Ahnert, F. (Ed.) *Einführung in die Geomorphologie*. Stuttgart: UTB, pp. 396–413.
- Schwardt, M., Köhn, D., Wunderlich, T., Wilken, D., Seeliger, M., Schmidts, T., et al. (2020) Characterization of silty to fine-sandy sediments with SH waves: full waveform inversion in comparison with other geophysical methods. *Near Surface Geophysics*, 18(3), 217–248. <https://doi.org/10.1002/nsg.12097>
- Scott, D.B. & Hermelin, J.O.R. (1993) A device for precision splitting of micropaleontological samples in liquid suspension. *Journal of Paleontology*, 67(01), 151–154. <https://doi.org/10.1017/S0022336000021302>
- Scott, D.B., Mediali, F.S. & Schafner, C.T. (2001) *Monitoring coastal environments using foraminifera and thecamoebian indicators*. Cambridge: University Press Cambridge. [10.1017/CBO9780511546020](https://doi.org/10.1017/CBO9780511546020)
- Sen Gupta, B.K. (1999) *Modern Foraminifera*. Heidelberg: Springer.
- Stanjek, H., Fassbinder, J.W.E., Vali, H., Wägele, H. & Graf, W. (1994) Evidence of biogenic greigite (ferrimagnetic Fe<sub>3</sub>S<sub>4</sub>) in soil. *European Journal of Soil Science*, 45(2), 97–103. <https://doi.org/10.1111/j.1365-2389.1994.tb00490.x>
- StatSoft, I. (2011) *STATISTICA für Windows (Software-System für Datenanalyse)*, Version 10.0. Tulsa, OK: StatSoft, Inc.
- Tisnérat-Laborde, N., Paterne, M., Métivier, B., Arnold, M., Yiou, P., Blamart, D. & Raynaud, S. (2010) Variability of the northeast Atlantic Sea surface  $\Delta^{14}\text{C}$  and marine reservoir age and the North Atlantic Oscillation (NAO). *Quaternary Science Reviews*, 29(19–20), 2633–2646. <https://doi.org/10.1016/j.quascirev.2010.06.013>
- UNESCO – United Nations Educational, Scientific and Cultural Organization. (2009) Natural properties - New Nominations - The Wadden Sea (Germany, Netherlands), Decision 33 COM 8B.4. Available at: <https://whc.unesco.org/en/decisions/1946> [accessed 29 October 2020].
- Verhegge, J. & Delvoie, S. (2021) Direct push, in situ video imaging of buried prehistoric landscapes in soft soils: First results in the polders, coversands, and loess belt of Belgium. *Geomorphology*, 373, 107483. <https://doi.org/10.1016/j.geomorph.2020.107483>
- Verhegge, J., Storme, A., Cruz, F. & Crombé, P. (2021) Cone penetration testing for extensive mapping of deeply buried Late Glacial covers and landscape paleotopography. *Geoarchaeology*, 36(1), 130–148. <https://doi.org/10.1002/gea.21815>
- Vos, P.C. & Knol, E. (2015) Holocene landscape reconstruction of the Wadden Sea area between Marsdiep and Weser: Explanation of the coastal evolution and visualisation of the landscape development of the northern Netherlands and Niedersachsen in five palaeogeographical maps from 500 BC to present. *Netherlands Journal of Geosciences*, 94(2), 157–183. <https://doi.org/10.1017/njg.2015.4>
- Vött, A., Handl, M. & Brückner, H. (2002) Rekonstruktion holozäner Umweltbedingungen in Akarnanien (NW-Griechenland) mittels Diskriminanzanalyse von geochemischen Daten. *Geologica et Palaeontologica*, 36, 123–147.
- Walther, J. (1894) Einleitung in die Geologie als historische Wissenschaft. In: *Lithogenesis der Gegenwart*, Vol. 3. Jena: G. Fischer, pp. 535–1055.

- Wegener, T. (1931) Vorläufige Mitteilung über Studien im nordfriesischen Wattgebiet. *Centralblatt für Mineralogie, Geologie Und Paläontologie*, 1931, 193–201.
- Wheeler, A.J., Oldfield, F. & Orford, J.D. (1999) Depositional and post-depositional controls on magnetic signals from saltmarshes on the north-west coast of Ireland. *Sedimentology*, 46(3), 545–558. <https://doi.org/10.1046/j.1365-3091.1999.00236.x>
- Wilken, D. & Rabbel, W. (2012) On the application of Particle Swarm Optimization strategies on Scholte-wave inversion. *Geophysical Journal International*, 190(1), 580–594. <https://doi.org/10.1111/j.1365-246X.2012.05500.x>
- Willmann, R. (1989) *Muscheln und Schnecken der Nord- und Ostsee*. Melsungen: Neumann-Neudamm.
- Wunderlich, T., Fischer, P., Wilken, D., Hadler, H., Erkul, E., Mecking, R., et al. (2018a) Constraining electric resistivity tomography by direct push electric conductivity logs and vibrocores: an exemplary study of the Fiume Morto silted riverbed (Ostia Antica, western Italy). *Geophysics*, 83(3), B87–B103. <https://doi.org/10.1190/geo2016-0660.1>
- Wunderlich, T., Petersen, H., Attia al Hagrey, S. & Rabbel, W. (2013) Pedophysical models for resistivity and permittivity of partially water-saturated soils. *Vadose Zone Journal*, 12, 21–39. <https://doi.org/10.2136/vzj2013.01.0023>
- Wunderlich, T., Wilken, D., Erkul, E., Rabbel, W., Vött, A., Fischer, P., et al. (2018b) The river harbour of Ostia Antica-stratigraphy, extent and harbour infrastructure from combined geophysical measurements and drillings. *Quaternary International*, 473, 55–65. <https://doi.org/10.1016/j.quaint.2017.07.017>

**How to cite this article:** Hadler, H., Vött, A., Willershäuser, T., Wilken, D., Blankenfeldt, R., von Carnap-Bornheim, C. et al. (2021) Automated facies identification by Direct Push-based sensing methods (CPT, HPT) and multivariate linear discriminant analysis to decipher geomorphological changes and storm surge impact on a medieval coastal landscape. *Earth Surface Processes and Landforms*, 46(15), 3228–3251. Available from: <https://doi.org/10.1002/esp.5232>